J. Appl. Comput. Mech., xx(x) (2026) 1-22
DOI: 10.22055/jacm.2026.49245.5832

ISSN: 2383-4536
jacm.scu.ac.ir

Shahid Chamran University of Ahvaz

Journal of Applied and Computational Mechanics

Research Paper

Numerical Investigation on a Novel Solar-Based Cogeneration System for Sustainable Power, Heat, and Freshwater Production in Remote Residential Buildings

Mohammad Bostani[1], Roohollah Rafee[2], Saman Rashidi[1], Guiqiang Li[3]

[1] Department of Energy, Faculty of New Sciences and Technologies, Semnan University, Semnan, Iran

[2] Faculty of Mechanical Engineering, Semnan University, Semnan, Iran

[3] Department of Thermal Science and Energy Engineering, University of Science and Technology of China, 96 Jinzhai Road, Hefei 230026, People's Republic of China

Received April 06 2026; Revised July 02 2026; Accepted for publication September 03 2026.
✉ Corresponding author: R. Rafee (Rafee@semnan.ac.ir)

Abstract. Building operations consume 30% of the world's energy and cause 26% of the associated emissions, while domestic water use accounts for 12% of global freshwater withdrawals. Renewable, solar-driven multi-generation systems can efficiently provide electricity, heat, and freshwater, especially for small, off-grid, remote households, addressing energy and water scarcity while improving sustainability and living quality. In this study, a novel cogeneration system for the generation of freshwater and energy, specifically tailored for applications in remote areas, is designed for the first time. This cogeneration system integrates a photovoltaic-thermal collector, a salt gradient solar pond, and a stepped solar still. The cogeneration system can produce an average of 4.026 MWh of electricity, 6.972 m^3 of fresh water, and 37.99 MWh of heat annually. The proposed system also produces at least daily values of 12.5 L of fresh water, 67.63 kWh of heat, and 6.284 kWh and 12.14 kWh of electricity in the cold and hot seasons, respectively. The system can produce 58.51 liters of fresh water, 7.123 kWh of electricity, and 68.425 kWh of heat on its first day of operation (April 1). Interestingly, 21.68 liters of freshwater and 17.98 kWh of heat were produced during the night.

Keywords: Cogeneration system; Freshwater; Solar energy; Electricity; Heat generation.

1. Introduction

The world's population has more than quadrupled, and global water consumption has increased by 600%. Among the various decentralized water treatment technologies, solar stills (SS) have emerged as a particularly attractive solution for remote and resource-limited regions due to their simplicity, low maintenance requirements, and reliance on abundant and free solar energy [1]. These systems operate based on evaporation and condensation [2]. Although the maintenance and operation costs of this system are low, it has low efficiency and is not suitable for high freshwater production capacities [3]. Consequently, substantial research efforts have been devoted to developing innovative strategies to enhance both the efficiency and freshwater yield of these systems. Goshayeshi et al. [4] systematically compared three distinct absorber geometries—semicircular, triangular, and rectangular—and demonstrated that dispersing graphene oxide nanoparticles into paraffin significantly improves thermal conductivity. Their results showed that the semicircular absorber, combined with nano-enhanced PCM, increased daily freshwater productivity by 20% and 10% relative to rectangular and triangular absorbers, respectively. This work clearly establishes that hybridizing nanomaterials with geometric optimization of the absorber plate is a highly effective strategy for performance enhancement. Esmaeili and Sheikholeslami [5] employed a rigorous computational fluid dynamics (CFD) approach to optimize both the glass cover geometry and the internal flow dynamics of a single-basin solar still. Their numerical analysis revealed that a conical glass cover outperforms trapezoidal designs, yielding an 8.44% increase in freshwater production. More notably, the incorporation of an internal circular baffle with an optimal radius (baffle-to-cover radius ratio = 0.8) into the conical configuration led to a 30.6% improvement in distillate output compared to the worst-performing trapezoidal design. This study compellingly demonstrates that vapor circulation patterns can be effectively managed through geometric and flow-control elements without the need for any material additives. Asadabadi and Sheikholeslami [6] investigated the synergistic effect of hollow circular copper fins and glass wool insulation on a pyramid-shaped SS. By increasing the number of fins from 81 to 144 and adding 3 cm of insulation, they achieved a daily freshwater productivity of 5.33 L/m² — a 62.5% improvement over a conventional SS — while simultaneously reducing the cost per liter by 27.33%. In a recent study [7], thermoelectric modules were incorporated into a SS to boost its overall performance. When compared to a conventional SS, the thermoelectric-integrated

Published online: September 15 2026

design showed clear improvements in both energy and exergy terms. Annual freshwater production reached 698.57 L per square metre, which is 41.2 % higher than that of the traditional still.

The unit annual benefit increased by 51 USD (also 41.2 %), and the benefit-to-cost ratio was 6.8 times higher. The cost per litre of distilled water dropped by 5.1 % to 0.037 USD. Furthermore, the modified system outperformed the conventional one in environmental, exergoenvironmental, exergoeconomic and enviroeconomic indicators, while reducing CO_2 emissions by 28.2 %. Prakash and Kumar [8] carried out an experimental comparison between a modified concatenated stepped solar still (MCSSS) and a simple version of the same design. The modified unit included internal and external reflectors as well as a cooling arrangement for the glass cover. Both stills had a basin area of 0.25 m² and were fed with tap water at 50 ml/min. The MCSSS yielded 3.43 litres of clean water per day, which is nearly 19 % more than the output from the simple still. The modified still also showed higher convective and evaporative heat transfer coefficients, by roughly 15 % and 11.5 %, respectively. Its energy efficiency reached 41.6 % and exergy efficiency 14.5 %, both significantly better than those of the simple unit. In addition, the payback period was shorter by about 1.3 months, and the carbon credits earned were higher. Taheri Mousavi [9] experimentally looked into how the shape of the absorber plate and the water flow rate affect the performance of a hemispherical solar still. Three different absorber designs were tested: a conical one, a funnel-shaped one, and a funnel-shaped one with stepped surfaces. The experiments were run at flow rates of 0.033, 0.066, and 0.1 kg/s. The best results came from the funnel-stepped design at the lowest flow rate of 0.033 kg/s. This configuration delivered an average daily freshwater output of 4.61 L per square metre, with a thermal efficiency of 42 %.

Compared to the conical absorber, which only produced 2.84 L/m²/day at 25 % efficiency, the funnel-stepped design improved productivity by 62 % and thermal efficiency by 67 %. A cost analysis also showed that the funnel-stepped still was more economical than the other two designs. The study clearly demonstrates that changing the absorber geometry, particularly by adding stepped surfaces to a funnel shape, can significantly boost the performance of hemispherical solar stills for small-scale desalination. Pandey and Naresh [10] built two pyramid solar stills and tested them side by side in Surat, India. One was a conventional design, and the other was modified by attaching a pulsating heat pipe to passively transfer extra heat into the basin. They ran experiments at four different water depths and found that the best performance for both stills occurred at a depth of 2 cm. At this depth, the modified still produced 4.10 L of fresh water per square metre per day, while the conventional one gave 3.05 L/m²/day. The heat pipe improved the yield by about 34 % at the same depth. Energy and exergy efficiencies were also better for the modified still, with gains of roughly 25 % and 29 %, respectively. The cost per litre dropped by around 13 %, and the modified still could offset nearly 18.8 tons of CO_2 emissions over its working life. The photovoltaic-thermal (PV/T) system, through its inherent cogeneration of electricity and heat within a single compact unit, effectively decouples energy supply from the electrical grid and fossil fuels, while its structurally simple design ensures high reliability and low-maintenance operation in remote, off-grid areas [11-12]. The incorporation of SSs with these systems is becoming more common, and research is continuing to enhance their efficiency and cogeneration of power and freshwater [13]. Mohtasim et al. [14] developed and experimentally investigated a PV/T system integrated with a modified pyramid SS. The system delivers heated fluid from a PVT/hybrid nano-PCM with fins (PVT/HNPCM/Fin) setup directly to the solar still basin to enhance evaporation. The modified still incorporates hollow circular fins, a black sand sensible heat storage layer, hybrid nano-PCM (paraffin wax with Al_2O_3 and ZnO nanoparticles), and sponges, while the PV/T loop utilizes a serpentine copper pipe at a flow rate of 0.0021 kg/s. The integrated system achieved a freshwater yield of 4.109 L/m²/day, with a cost per liter of only $0.01495 (a 94.13% reduction compared to the local market price). Overall exergy efficiencies reached nearly 2% for the solar still and 94% for the PV/T system at peak solar noon. A comprehensive 11E sustainability analysis revealed that the system can mitigate approximately 6.98 tons of CO_2 emissions over its lifetime. Rajesh and Chiranjeevi [15] experimentally examined a combined power and desalination system that integrates a stepped SS with a PV/T module having a serpentine-type thermal absorber. Unlike conventional designs, their setup uses the waste heat from the PV/T unit to preheat the saline feed water before it enters the SS. The freshwater yield reached 3.46 L/m² per day, with an average electrical efficiency of 14.84 % for the PV/T panel. The exergy efficiency was found to be 18.5 %, and the cost of producing one litre of distilled water was estimated at 0.07 USD. While these systems have the potential to be used as a cogeneration system for power, heat, and freshwater, studies show that a considerable amount of thermal energy, especially heated brine from the desalination process, is wasted. In addition, the high dependence of such systems on thermal energy storage units leads to increased overall system costs and reduced operational reliability. Conventional methods for storing and utilizing solar thermal energy face significant limitations due to high costs and technical complexities, which hinder the widespread deployment of such systems. The use of a salt gradient solar pond (SGSP) as a reliable system for the simultaneous collection and storage of solar energy is considered a rational and cost-effective solution. Moreover, the absence of integrated residential cogeneration systems for electricity, heat, and freshwater has left such systems largely unexplored, despite their potential to enhance energy and water security and improve the quality of life in small, remote households [11].

In this study, a novel cogeneration system for freshwater and energy production, specifically tailored for small-scale applications in remote areas, is designed for the first time. This cogeneration system integrates a PV/T, an SGSP, and a SSS. This system enhances the performance of energy and water production by effectively utilizing the stored thermal energy, thereby improving the performance of the SSS. Moreover, this approach offers significant economic and environmental advantages due to the effective use of solar irradiation resources and the reduction of thermal losses. Among these advantages is the capability for continuous (24-hour) production of heat and freshwater, effectively meeting heating and potable water demands even during nighttime hours. The solar cogeneration system for freshwater, electricity, and heat will be designed to meet the needs of a four-member household under the climatic conditions of Semnan.

2. Problem Statement

As illustrated in Fig. 1, brackish water is preheated twice, first by absorbing heat generated by the PV/T and then by a SGSP, before entering the SSS. This process increases the evaporation rate, which in turn leads to a higher production of freshwater by the SSS. Since the saline water exiting the SSS has absorbed heat in three stages, it retains a high temperature and can be utilized to supply the thermal energy needed for domestic hot water. The electrical energy supply is also provided by the PV/T system. Based on the thermal load demand, the dimensions of the SGSP can be designed in such a way that the stored heat can be utilized at night for the production of freshwater and hot water. In this system, it is assumed that heat losses along the pipes are negligible and can be disregarded. The saline water flows into the system continuously and uniformly, and the processes of evaporation and condensation also occur steadily and continuously. It is also assumed that all the generated vapor in the SSS is completely condensed and converted into freshwater.

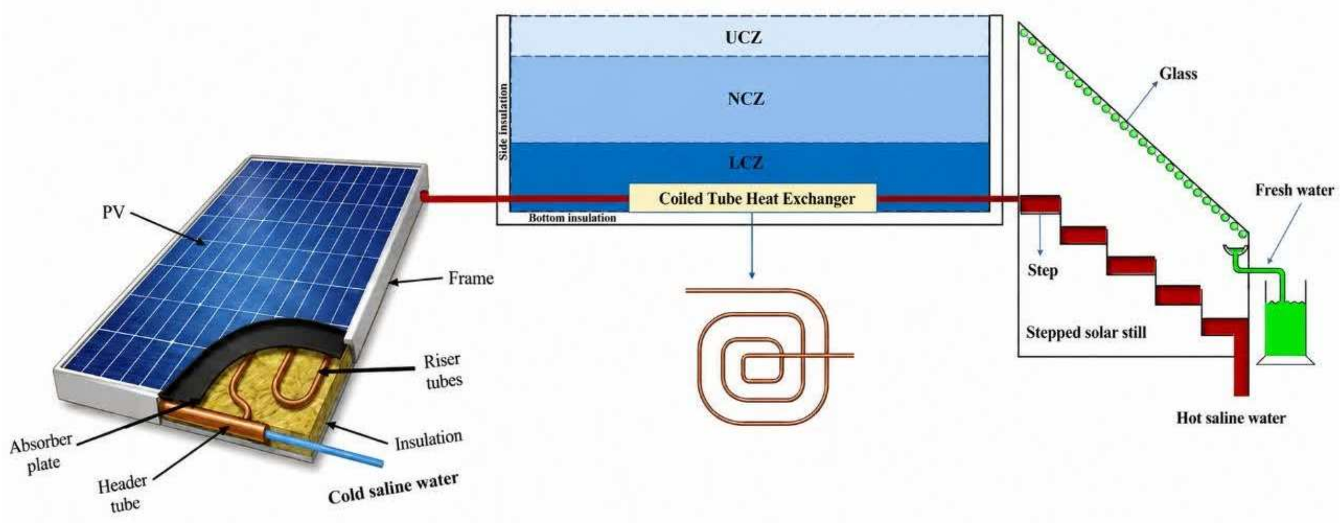

Fig. 1. Conceptual representation of the developed system.

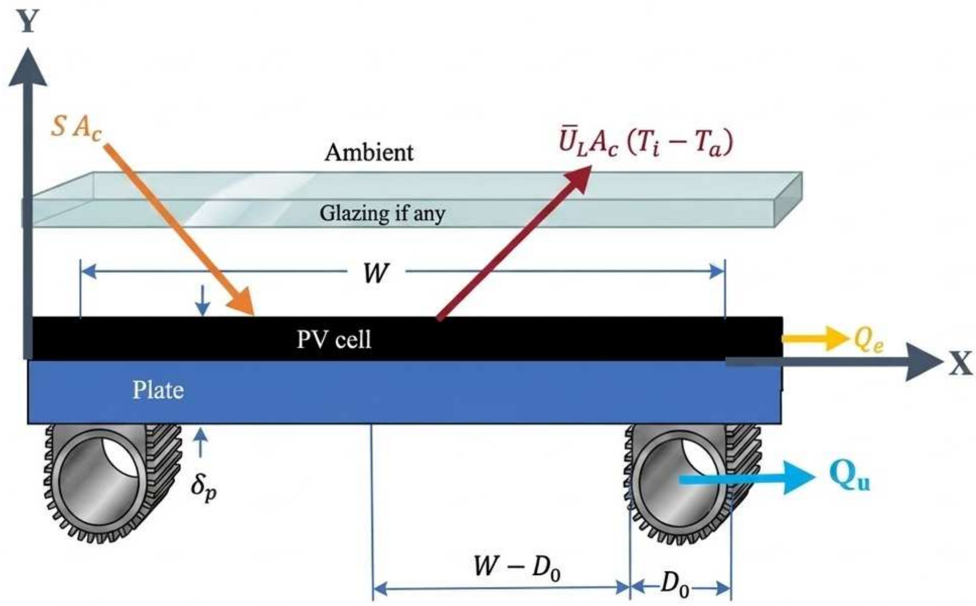

Fig. 2. Representation of the structure and energy balance of the flat-plate PV/T collector.

3. Mathematical Model

In this part, the mathematical framework and the key equations of the SGSP, the SSS, and the PV/T collector will be presented. The governing equations will be used for the numerical simulation of each part of the system.

3.1. PV/T

The flat-plate PV/T collector can be analyzed using a method similar to that employed for conventional flat plate collectors (FPCs), which involves applying the basic FPC analysis model [16], with modifications proposed by Florschuetz [17], and Charalambous et al. [18]. According to Fig. 2, the energy equation for the PV/T collector is as follows [17]:

Radiation absorbed by PV/T = Electrical output of the PV/T + Thermal energy gained by PV/T + Overall thermal loss rate from PV/T to ambient:

$$SA_c = [Q_e + Q_u + \bar{U}_L A_c (T_i - T_a)] \tag{1}$$

In PV/T collectors, heat loss to the ambient through various ways of heat transmission is unavoidable. In PV/T collectors, a corrected overall heat loss coefficient ($\bar{U}_L$) is used to account for the reduction in thermal losses due to the extraction of the electricity. This coefficient is a complex function of the collector's structure and its operating conditions and can be calculated using the equations provided by Kalogirou [19]. In the above equation, S represents the absorbed solar irradiation. Solar irradiation, after passing through the transparent cover and undergoing reflection, refraction, and absorption, is captured by the absorber surface and changed into thermal energy [20]. This energy can be determined by [19]:

$$S = I_t(\tau_g \alpha_p) \tag{2}$$

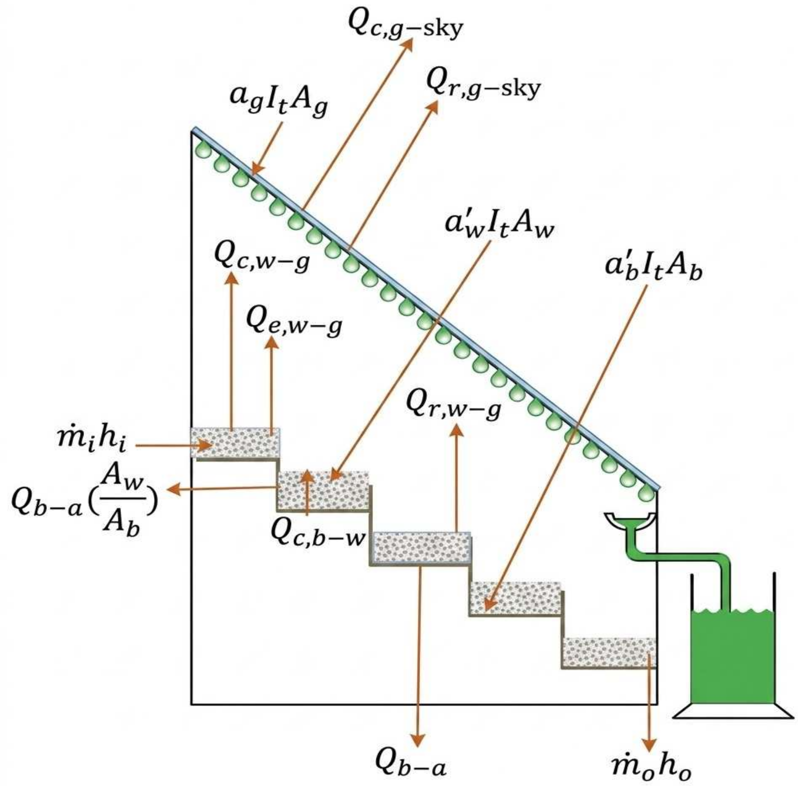

Fig. 3. Energy flow diagram in a SSS.

The transmissivity of the cover in a PV/T collector can be accurately estimated by separately analyzing reflection-refraction and absorption, using the equations reported by Sukhatme [21]. The collector efficiency factor, defined in [22], is calculated by incorporating the characteristics of the solar cell, using the relation provided by Charalambous et al. [18]. The forced convection heat transfer coefficient inside the tube can be calculated using the equations provided by Holman [23].

3.2. SSS

For the SSS, the equations proposed by Tiwari [24] are employed, with the modification that the energy associated with mass flow into and out of the system is also considered. Because the glass cover and absorber plate are thin and therefore have low thermal inertia [24], the heat capacities of the glass cover, absorber plate, and insulation at the bottom and sides are assumed to be negligible. The temperatures of the absorber plate, water, and glass cover at any time can be obtained by solving the energy balance equations for these three components of the SSS. As shown in Fig. 3, the energy balance equations for the different elements of the SSS are given as follows [24]:

- Absorber plate (steps):

$$a'_b I_t A_b = Q_{c,b-w} + \left[Q_{b-a} + Q_{b-a}\left(\frac{A_w}{A_b}\right)\right] \tag{3}$$

- Water mass:

$$a'_w I_t A_w + Q_{c,b-w} + \dot{m}_i h_i = \dot{m}_o h_o + Q_{r.w-g} + Q_{e,w-g} + Q_{c.w-g} + (MC_p)_w \frac{dT_w}{dt} \tag{4}$$

- Glass covers:

$$\alpha_g I_t A_g + Q_{r.w-g} + Q_{e,w-g} + Q_{c.w-g} = Q_{r.g-sky} + Q_{c.g-sky} \tag{5}$$

where a'_w and a'_b represent the fractions of solar radiation absorbed by the saline water and the steps, respectively, and are calculated using Eqs. (6) to (7) [24]:

$$a'_w = (1-\alpha_g)\tau_g \alpha_w \tag{6}$$

$$a'_b = (1-\alpha_g)\tau_g \tau_w (1-\alpha_w)\alpha_b \tag{7}$$

The hourly water evaporation rate, accounting for the energy associated with mass flow into and out of the system, is obtained from Eq. (8) [24]:

$$Q_{e,w-g} = \dot{m}_i h_i - \dot{m}_o h_o + (a'_w + a'_b) I_t A_b - U_{LS}(T_w - T_a) A_b \tag{8}$$

The mass balance of water in the SSS is also given by the following equation:

$$\dot{m}_o = \dot{m}_i - \dot{m}_{evap} - \dot{M}_w \tag{9}$$

The convective heat transfer rate from the bottom of the steps to the saline water, the heat loss rates from the bottom and side surfaces of the steps to the ambient, the heat loss rate from the glass to the ambient, and the heat transfer rate from the saline water to the glass can be calculated using the equations provided by Tiwari [24].

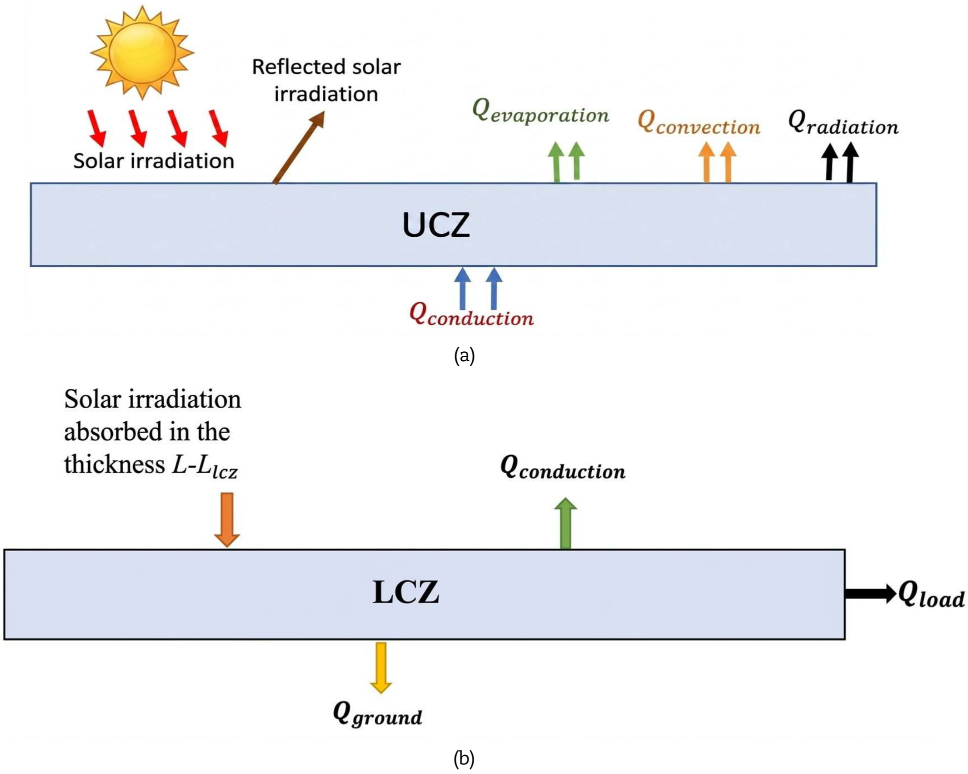

Fig. 4. Energy transfer for (a) UCZ and (b) LCZ.

3.3. SGSP

For the SGSP, the equations presented by Sayer et al. [25] are used, with the modification that the energy extracted from the system is also taken into account. The equations are derived by formulating the energy conservation equations for the LCZ and UCZ. Certain simplifications and assumptions are made due to the complexity involved [25]. According to Fig. 4, the energy conservation equation for each layer of the SGSP is as follows [25]:

- LCZ:

$$\rho_{lcz} L_{lcz} C_{p,lcz} A_{lcz} \left(\frac{\partial T_{lcz}}{\partial t}\right) = \left[(I)_{x=L-L_{lcz}}\right] A_{lcz} - Q_{cond} - Q_{load} - Q_{ground} \tag{10}$$

- UCZ:

$$\rho_{ucz} L_{ucz} C_{p,ucz} A_{ucz} \left(\frac{\partial T_{ucz}}{\partial t}\right) = Q_{cond} + \left[(I)_{x=0} - (I)_{x=L_{ucz}}\right] A_{ucz} - Q_{losses,ucz} \tag{11}$$

When solar energy reaches an SGSP's surface, some reflects skyward while the rest enters the pond [26]. To analyze SGSP performance, we first determine how much incoming sunlight reflects off, absorbs into, or passes through the water layers. The solar irradiation flux at depth x is obtained from Eq. (12) [25]:

$$I_x = \tau_r I_t \tau_\alpha \tag{12}$$

in which τ_α and τ_r are the transmissivities of absorption and refraction-reflection at SGSP surface, both of which can be estimated using the equations reported by Sukhatme [21]. The conduction heat transmission from the LCZ to the UCZ, the SGSP surface heat loss, and the heat losses from the LCZ to the ground can be calculated using the equations provided by Sayer et al [25]. Heat extraction from the LCZ is carried out using a heat exchanger consisting of a single long coiled tube located at the bottom of the SGSP .The heat transmission fluid, by passing through this tube, absorbs heat from the LCZ. The amount of useful heat obtained and the temperature of the outlet fluid from the SGSP heat exchanger can be calculated using equations provided by Jaefarzadeh [27]. The forced convective heat transmission coefficient inside the tube and the natural convection heat transfer coefficient of the fluid surrounding the heat exchanger tubes can be calculated using the equations provided by Holman [23]. The thermophysical properties used in the calculation of the above coefficients vary over time and are determined using Perry's handbook [28] and equations provided by Verma and Das [29].

4. Validation

In this section, the numerical models developed for simulating the performance of each system component will be validated.

4.1. Validation of the PV/T model

The research of Charalambous et al. [18] was selected to validate the model. Charalambous et al. [18] investigated the performance of a PV/T collector with a header-riser configuration experimentally and theoretically. The operating conditions and specifications of this collector are given in complete detail by Charalambous et al. [18]. In this work, a model was created in EES software, and the results derived from the present model were assessed against the theoretical and experimental results of their research. Other parameters required for validating this model in the EES software can also be seen in Table 1.

Table 1. Parameters related to PV/T modeling.

Parameters	Values	Parameters	Values
ε_g [20]	0.88	k_{back} [30]	0.018 W/m.K
U_e [19]	2 W/m²K	C_p [20]	4.179 kJ/kg.K

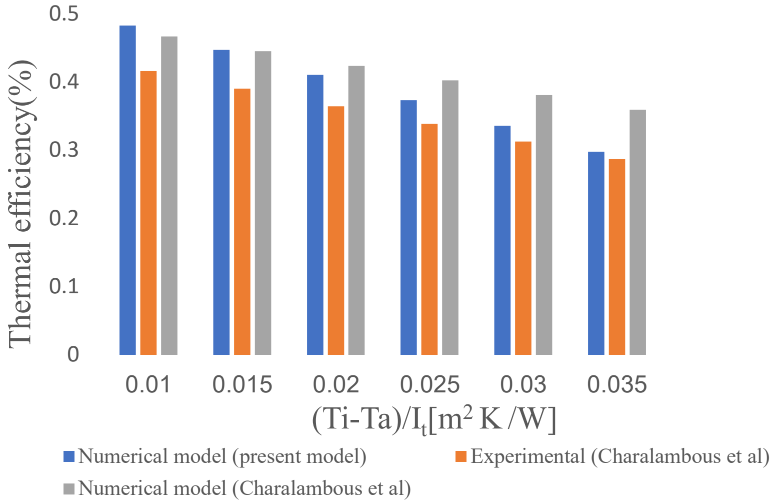

Fig. 5. Comparison of thermal efficiency obtained from the present model with the research of Charalambous et al. [18].

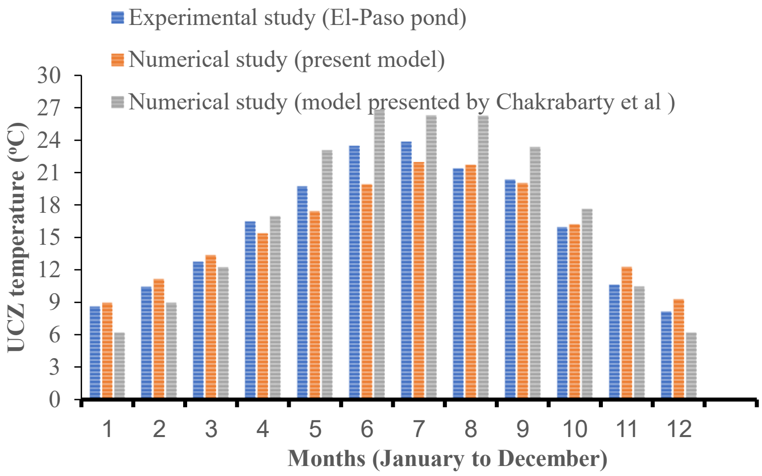

(a)

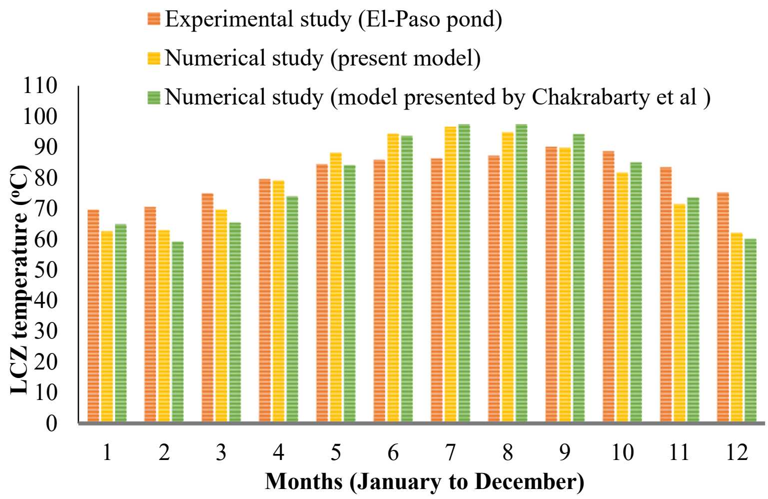

(b)

Fig. 6. Validation of temperature predictions: current modeling approach versus Chakrabarty et al. technique [26] against experimental records from El Paso SGSP [31], (a) UCZ, and (b) LCZ.

As shown in Fig. 5, the findings of the model align well with those presented by Charalambous et al. [18]. The results of the present simulation are more precise than the model developed by Charalambous et al. [18], as the root mean square deviation for the present model and the Charalambous et al. model [18] compared to the experimental results are 0.04526% and 0.06181%, respectively.

4.2. Validation of the SGSP model

A time dependent simulation has been performed by EES software to investigate the performance of the SGSP. Various approaches are applied to solve the equations governing heat transmission in a SGSP. In this research, the finite difference technique has been used. For validation, the results are validated against available experimental data from the El Paso SGSP [28] and the numerical results given by Chakrabarty et al. [26]. The relative features, initial boundary conditions, and climatic data for the El Paso SGSP are provided fully detailed by Chakrabarty et al. [26] and Lu et al. [31]. The SGSP performance was evaluated monthly and a time step of 90 hours was considered for the simulation during this period. Simulations were conducted to predict the LCZ temperature and the UCZ temperature over a year. Figure 6 shows that temperature changes over time in each layer closely match experimental measurements. Our computational framework demonstrates superior precision compared to Chakrabarty et al.'s prior simulation approach [26] because RMS error magnitudes for LCZ temperature calculations are 7.95°C (current model) versus 8.79°C (Chakrabarty et al. [26]), indicating superior precision in our methodology.

4.3. Validation of the SSS model

In this section, for validation purposes, an experimental test was conducted with a device built by Zarei et al. [32]. Figure 7 displays a view of the SSS. The top glass cover, with an area of 0.4968 m^2, also has a major role in the evaporation and distillation process. There is a 1 cm high edge and a 1 cm long gap at the end of each step to prevent overflow and to lengthen the water path. Other technical specifications of this device and measurement equipment are detailed by Zarei et al. [32]. The performance of the SSS, with an input flow rate of 3.26 kg per hour, was examined on December 27th under the climatic conditions of Semnan City from 10 AM to 3 PM. During the experiment, the inlet flow rate was kept constant. Every hour, important parameters such as the amount of freshwater production, solar irradiation, the temperature of the incoming saltwater to the SSS, the temperature of the outgoing saltwater, ambient temperature, glass temperature, wind speed, and the temperature of the saltwater on the steps were measured using measuring devices. The operational conditions of the experimental facility and the measured parameters in the conducted tests are illustrated in Fig. 8.

For validation, a model was created in EES software. Equation solutions were derived through algebraic transformation of derivatives using nodal analysis, which is called finite difference. The relevant equations were solved with a time step of 3600 seconds to calculate the outlet brine temperature and the produced freshwater flow rate. The parameters related to the model are given in Table 2. For 10:00 AM, the initial temperature of the saltwater on the steps is supposed to be equal to the ambient temperature. Subsequently, the final saline water temperature on the steps at each hour is considered as the initial saline water temperature for the following hour. It should be noted that the mass of saline water remaining inside the SSS each hour is 2.8 kg. Amount exceeding this value overflows and is discharged from the brine outlet. As shown in Fig. 8, the measured saline water temperatures on the last three steps and the brine outlet temperatures of the device are nearly identical, with a difference of less than one degree Celsius. Therefore, in the conducted modeling, the saline water temperature on the steps and the brine outlet temperature of the device are assumed to be the same. The parameters of saline water temperature on the steps and the rate of freshwater production were calculated and compared with experimental data. As observed in Fig. 9, the model results align with the experimental data. For the saline water temperature on the steps and mass of produced freshwater, the largest variation between the theoretical and experimental results is observed at 10:00 AM. As depicted in Fig. 9, unlike other hours of the day, the theoretical saline water temperature on the steps and the theoretical freshwater production are higher than those observed in the experimental results. Because at this hour, a large amount of solar energy is spent heating the steps and at the same time the steps are filled with salt water. Over time, after the steps are filled, freshwater production increases. This effect cannot be applied in the theoretical model, which could be one of the reasons for the difference between two results in the validation.

Fig. 7. View of the tested stepped-type solar still.

Table 2. Parameters related to SSS modeling.

Parameter	value	Parameter	value
α_w [33-34]	0.05	ε_w [35-38]	0.96
α_g [36-37]	0.05	α_p [38-41]	0. 95
ε_g [34-36]	0.88	τ_g [33-34]	0.9
τ_w [33-36]	0.95	$h_{c,b-w}$ [39-41]	135W/m^{2}K
h_b [37-39]	14 W/m^2 K	C_p [33]	4.190 kJ/kg.K

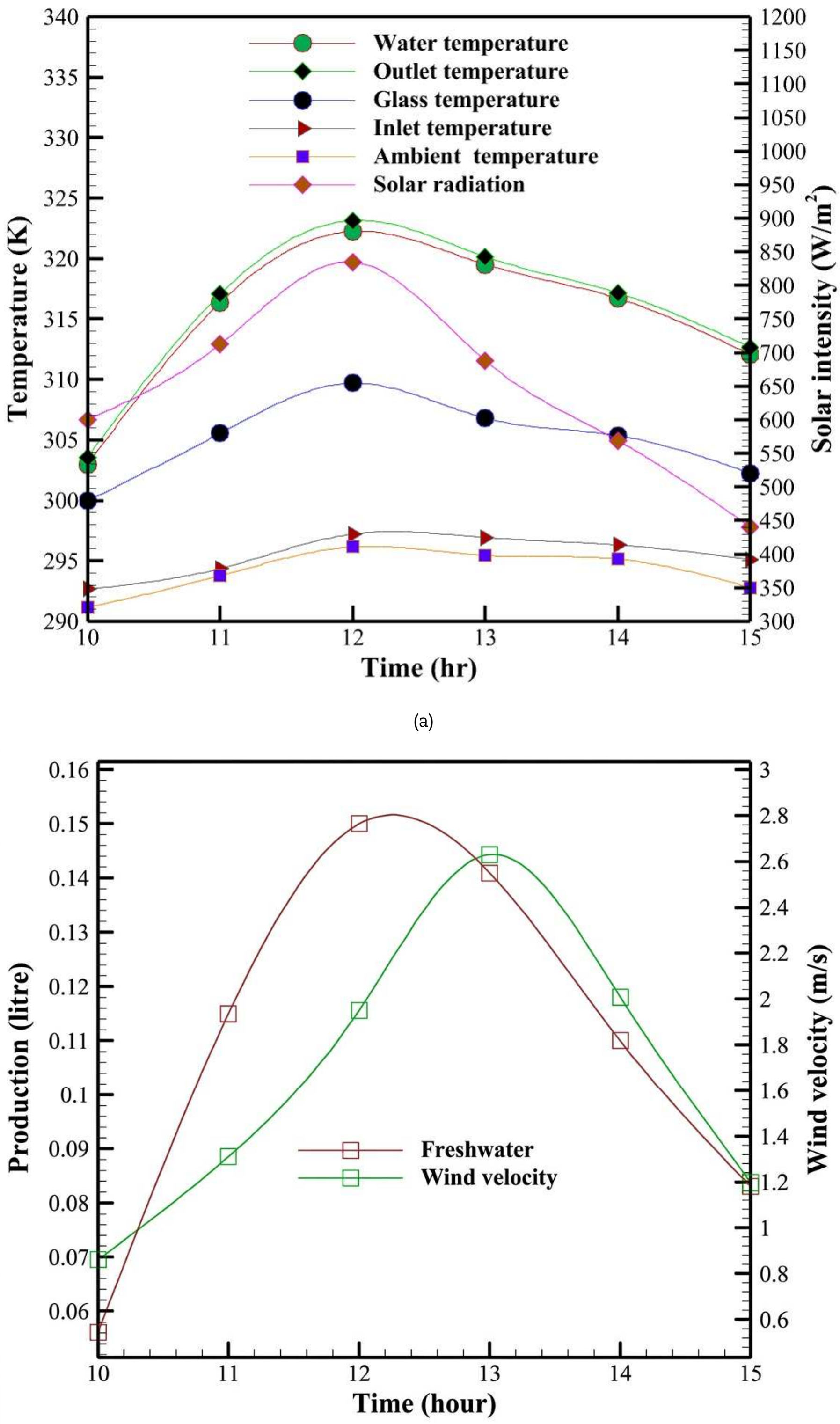

Fig. 8. Experimental results: (a) temporal variations of measured temperatures, (b) variations of freshwater production and wind velocity.

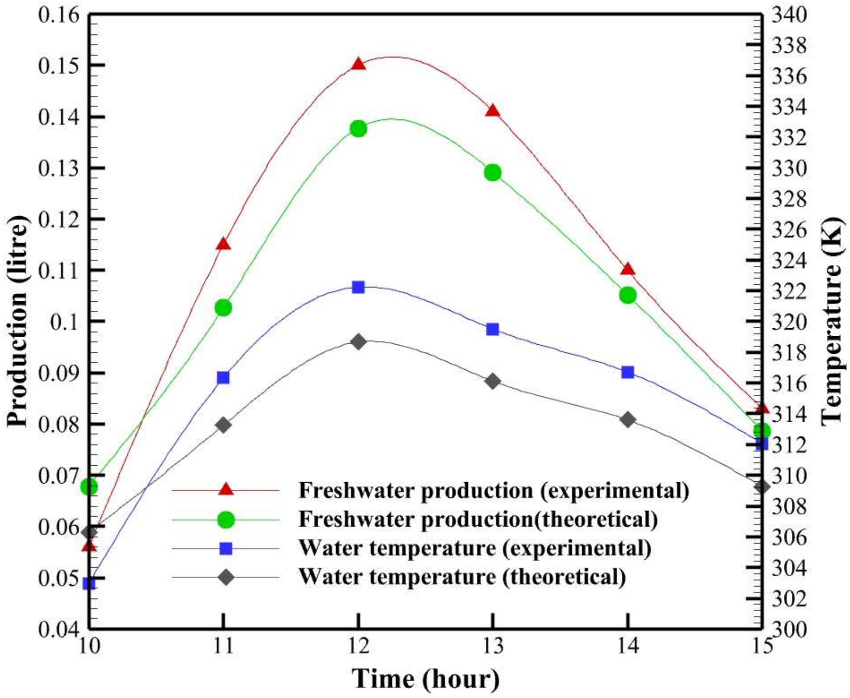

Fig. 9. Comparison of saltwater temperature on the steps and freshwater production in theoretical and experimental cases.

5. Design of the Solar Cogeneration System

The goal of this research is to design a solar cogeneration system for a four-person household in Semnan city. The flowchart of the solar cogeneration system design can be seen in Fig. 10. Weather data of Semnan city, including monthly average irradiation, temperature of the ambient, wind velocity, and humidity of air, were adopted from Meteonorm 7.3 software and are given in Table 3 [43]. The required electricity is also determined based on the operating hours of the devices and their power consumption. The power consumption of each electrical appliance and its operating time are shown in Table 4. The required heat can be estimated by considering the amount of heat needed for various activities. The mentioned system must have the capability to produce an average of 4.315 kWh and 11.455 kWh of electricity per day during the cold and warm seasons, respectively. From June to late September, the evaporative cooler consumes 7.140 kWh of electricity per day. The temperature of the hot water consumed in the domestic sector is assumed to be 333.15 K [44], and the cold water temperature is supposed to be equal to the ambient temperature. The dimensions of the cogeneration system must be designed to supply the essential heat for producing fresh water and hot water at a temperature of 333.15 K for the activities specified in Table 5. Utilizing the information presented in Table 5 about a domestic unit of four people and typical daily activities, which include two instances of food preparation, two occurrences of manual dishwashing, one shower per individual, and two hand-washings per individual each day, one can derive the small, middle, and high water consumption in liters per individual as depicted in Table 6. The scenario representing maximum consumption occurs when the daily shower for each individual is substituted with a bath for each individual.

Table 3. Climate data of Semnan city [43].

Month	Relative humidity (%)	Ambient temperature (K)	Solar irradiation on horizontal surface (W/m^2)	Solar irradiation on tilted surface (W/m^2)	Wind speed (m/s)
January	63.9	276.62	115.1	136.66	1.4
February	49.7	280.25	164	178.61	1.99
March	37.6	285.95	225.9	228.61	2.39
April	36.7	291.25	284.9	274.44	2.7
May	27.8	297.45	326.3	305.55	3.29
June	23.5	302.35	345.2	319.44	3.49
July	24.4	305.15	312.1	291.6	3.4
August	22.8	304.05	293	279.16	2.89
September	24.9	299.35	253.3	250.83	2.6
October	32.5	293.05	180.3	190.55	2.11
November	48.4	284.25	126.7	146.38	1.69
December	65.6	278.37	101.3	124.44	1.19

Table 4. Power consumption of electrical appliances [42].

Electrical Device	Nominal wattage (W)	Operating Duration
Refrigerator- Freezer	110	24
evaporative cooler	420	17
TV	105	2
Lighting	120	8
-	400	-

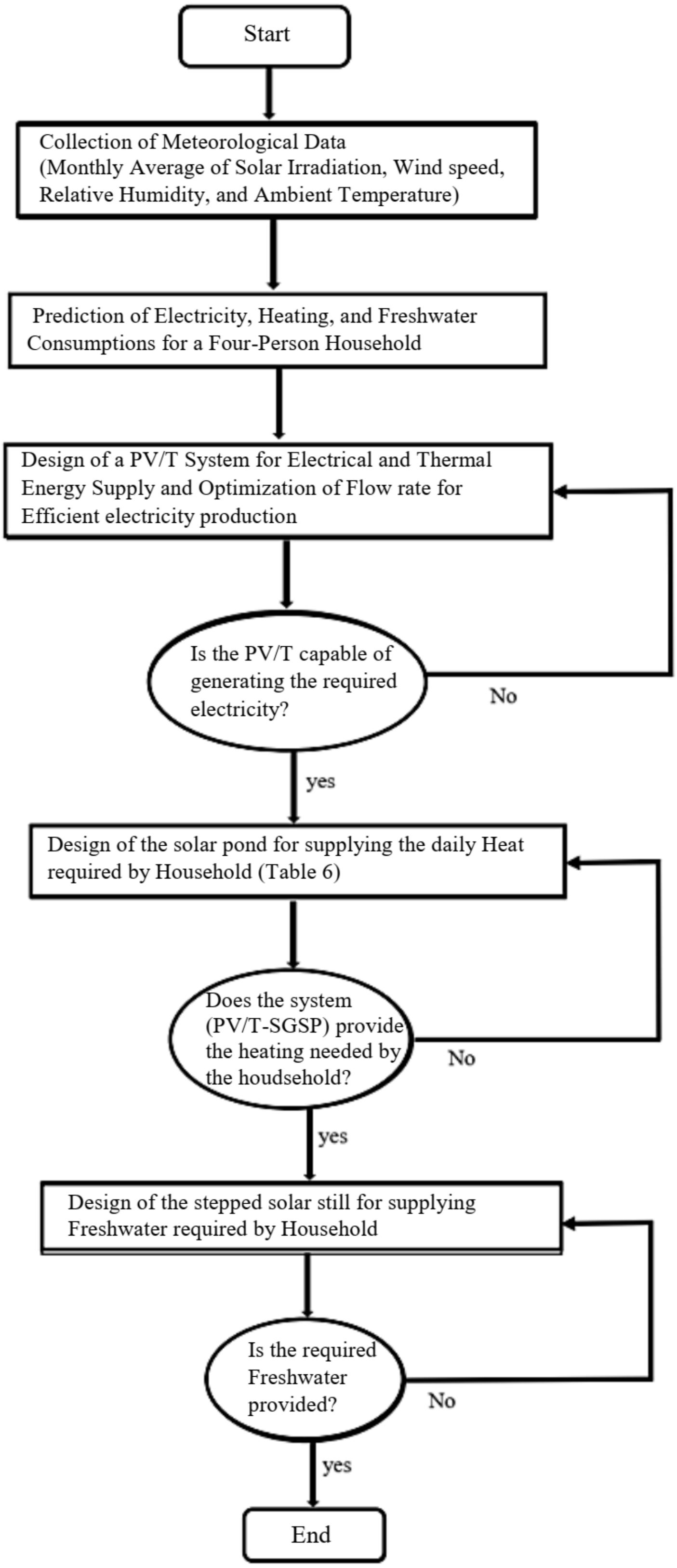

Fig. 10. Flowchart of the design process for solar cogeneration system.

Table 5. Residential hot water consumption for each activity [19].

Application	Consumption (litre/day)
Preparation of food	10-20
Dishwashing	12-18
Shower	10-20
Bath	50-70
Hand and face washing	5-15

Table 6. Daily Hot Water Requirements for a four-person family (Litere/person/day) [19].

Guideline	Low	Medium	high
Normal consumption	26	40	54
Maximum consumption	66	85	104

Table 7. PV/T specifications [18-20].

Parameter	Value	Parameter	Value
δ_a	0.005 m	ε_p	0.9
t/2	0.0025 m	α_P	0.86
k_{si}	84 W/m.K	L_s	1.96 m
δ_{si}	0.00035 m	δ_{glass}	4 mm
E	15 m^{-1}	w_c	0.97 m
k_{plate}	400 W/m.K	δ_{edge}	0.02 m
C_b	400 W/m.K	k_{edge} [46]	0.034 W/m.K
U_{ca}	200 W/m^2K	β_{ref}	0.003/K
T_{ref}	25°C	k_{back} [30]	0.018 W/m.K
η_{ref}	0.1	δ_{back}	0.05 m
D_h	0.04 m	β	35.6°
ε_g	0.88	N_c	11
w	0.04 m	D_i	0.02 m

The domestic hot water consumption for a four-person family with medium normal consumption is 160 liters per day. Therefore, a family of four person requires a maximum of 10.480 kWh of heat per day. Each person requires an average of 2.8 liters of fresh water per day for drinking and cooking, meaning a family of four needs 11.2 liters per day [45].

6. Results and Discussions

Here, the dimensions and performance of the components of the cogeneration system are discussed to meet the demand for energy and fresh water.

6.1. PV/T

To meet the electricity needs, a PV/T with a header-riser configuration was designed with the specifications presented in Table 7. The header-riser configuration has 157 copper riser pipes with a length of 1.88 m and a diameter of 0.025 m. In this configuration, there are two copper header pipes with a diameter of 0.04 m. The distance between the riser pipes is 0.04 m. The described configuration is connected to a copper plate with a thickness of 0.005 meters, which acts as a heat absorber. Polyurethane and polystyrene are used as back and side insulation, respectively. The water input flow rate is 80 kg/hr because, in addition to effectively cooling the photovoltaic panel and absorbing its heat, it must be able to provide the required freshwater production by absorbing sufficient heat from the SGSP. The concentration of saline water entering the system is 960 mg/L [29] and its thermophysical properties varied in all components of the cogeneration system at each time interval. The thermal and electrical performance of the PV/T is evaluated monthly, starting from April, in two configurations of unglazed and glazed. The reason for starting the system operation in April is that the SGSP can store more thermal energy for heating the PV/T outlet saline water during the winter and autumn seasons. As shown in Fig. 11, the electricity generated by the glazed collector is lower than that produced in the unglazed configuration. Since the glass cover reduces the performance of the PV panel due to increased optical losses and higher panel temperatures, it results in lower electricity generation. However, the glazed collector, due to reduced thermal losses from the PV panel surface to the environment, generates more heat compared to the unglazed configuration. Since the electricity supply is only provided by this part of the cogeneration system, the unglazed PV/T with higher electrical performance is selected. The unglazed PV/T with an area of 21 m² provides a minimum of 6.284 kWh/day and 12.14 kWh/day of electricity daily in the cold and warm seasons, respectively. It generates an average of 4.026 MWh of electricity annually. Therefore, this system generates an average of 1.58 MWh/year of electricity, higher than the yearly consumption (2.878 MWh/year).

The negligible variation in the outlet fluid temperature between June and July can be explained by the combined influence of solar irradiance, inlet fluid temperature, and wind-induced thermal losses. Although the solar irradiance in July is lower than that in June, leading to a reduction in PV cell and absorber temperatures, this effect is partially compensated by the higher ambient temperature in July. Since the inlet fluid temperature is assumed to be equal to the ambient temperature, the working fluid enters the collector at a higher temperature during July. Furthermore, the wind speed in June is approximately 0.5 m/s higher than in July. For an unglazed PVT collector, convective heat losses from the absorber surface are strongly dependent on wind speed. Therefore, the higher wind velocity in June enhances convective heat transfer to the surroundings and increases thermal losses from the collector. In contrast, the lower wind speed in July suppresses these losses and promotes heat retention within the collector. As a result, two competing mechanisms are observed: the lower solar irradiance in July tends to decrease the thermal energy absorbed by the collector, whereas the higher inlet fluid temperature and lower convective heat losses tend to increase the outlet fluid temperature. The combined effect of these opposing factors leads to a near-equilibrium thermal behavior, explaining why the outlet fluid temperatures in June and July remain very close despite the differences in meteorological conditions. This observation highlights that, for unglazed PVT collectors, the outlet fluid temperature is governed not only by solar irradiance but also by the balance between absorbed solar energy and environmental heat losses. Consequently, variations in ambient temperature and wind speed may significantly moderate the expected influence of irradiance on the collector thermal performance.

6.2. SGSP

The SGSP should be designed to provide sufficient heat to produce fresh water in the SSS as well as to produce hot water at appropriate temperatures for the activities listed in Table 5. The concentration of dissolved salts such as sodium chloride ranges from 20-30% at the pond bottom to near zero at the water surface [47]. Based on the above explanations, in the present work, the salt concentration in LCZ is considered to be 0.26 kg/L. A SGSP with an area of 10 m² and a depth of 1.1 m was designed, where the thicknesses of UCZ and LCZ were 0.1 m and 0.4 m, respectively. The NCZ is thicker and constitutes about half the thickness of the SGSP [21], so the thickness of the NCZ was considered to be 0.6 m. Reducing heat losses is an effective technique for enhancing the efficiency of SGSP, and using insulation under the SGSP to reduce heat loss to the ground can be effective in this regard. Glass wool with a width of 1.5 cm was used as insulation under the SGSP. The lateral walls of the SGSP are also fully isolated. The ground temperature is equal to the annual mean temperature of the ambient in that region; therefore, the ground temperature was also determined based on this point [48]. Other specifications of the SGSP are summarized in Table 8. During the simulation, it was observed that when the SGSP starts operating, no heat can be extracted from it because a considerable time is necessary for the heating of this volume of water.

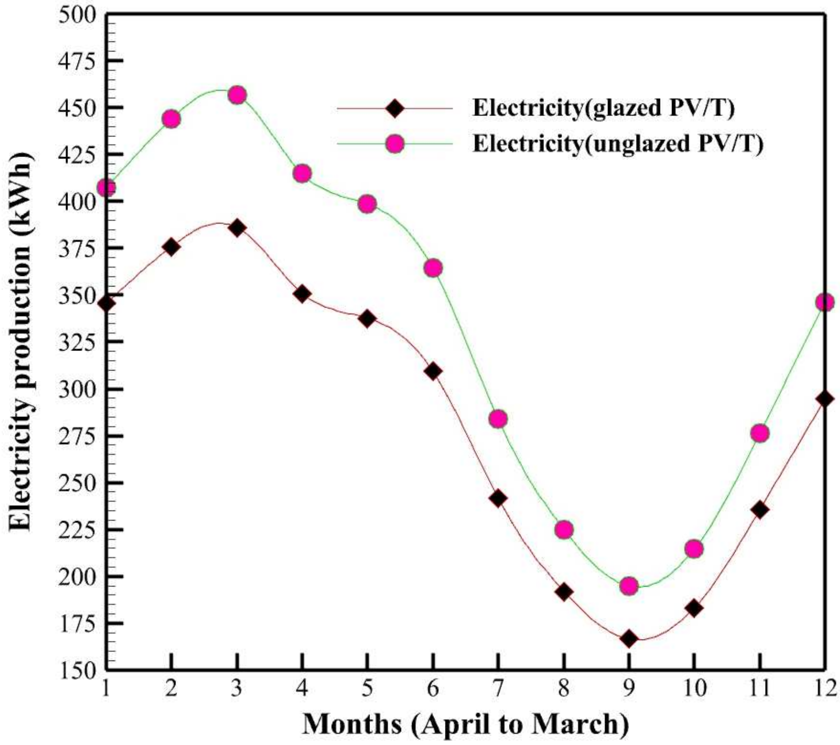

(a)

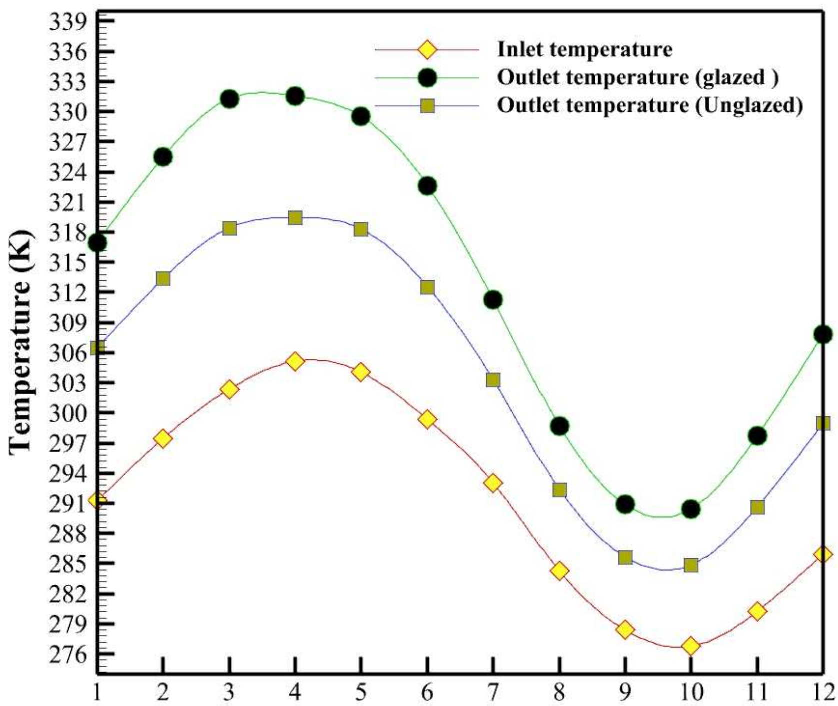

(b)

Fig. 11. Comparison of (a) electrical energy produced, (b) output temperature from PV/T in the unglazed and glazed case.

As a case study, the hourly performance of the SGSP from June 22 to June 25 was analyzed under the weather conditions presented in Fig. 12. The weather data for Semnan city on these days were extracted using the Meteonorm 7.3 software [43]. Initially, the performance of the SGSP was simulated for three days without heat extraction, and subsequently, the feasibility of heat extraction was evaluated. The mass rate of brine entering the SGSP heat exchanger is 80 kg/h, and its temperature is assumed to be ambient temperature. The initial temperatures of the LCZ and UCZ are supposed to be equal to the ambient temperature at 6:00 AM on June 22. As shown in Fig. 13, the LCZ temperature in the SGSP increases by an average of 6 to 7 °C per day. Since the UCZ is in contact with the surroundings, its temperature remains close to the ambient temperature and changes in a similar pattern. On June 25, the heat was extracted from the SGSP. As shown in Fig. 14, the SGSP demonstrated the ability to supply thermal energy both during the day and at night on June 25. This capability is particularly noticeable during hours without solar radiation. On this day, a 7 °C rise in the temperature of the LCZ was also observed. At 00:00 AM on June 26, the entering fluid temperature to the SGSP heat exchanger increased to 316 K, corresponding to the highest amount of heat extracted from the SGSP. Based on the above observations, if the SGSP is operated as part of the cogeneration system from the first day, it will extract heat from the PV/T system's outlet fluid, thereby reducing the overall thermal performance of the integrated system. Accordingly, it was decided that the SGSP would operate without heat extraction throughout February and March, allowing thermal energy to accumulate. The cogeneration system would then begin operation on April 1st. The initial temperatures of UCZ and LCZ were assumed to be equal to the ambient temperature during the month of February. After two months of operation, the LCZ and UCZ temperatures reached 286.99 K and 328.76 K, respectively. These values are considered as the initial temperatures of the UCZ and LCZ on the first day of cogeneration system operation (April 1st).

The monthly thermal performance of the SGSP coupled with the PV/T system was studied. As illustrated in Fig. 15, the highest outlet temperature from the SGSP heat exchanger occurs in June and July due to high ambient temperatures and solar irradiation. Even in January, the coldest month with an ambient temperature of 276.77 K, the SGSP performed effectively by more than doubling the saline water temperature exiting the PV/T collector. Throughout the year, the temperature of UCZ remains close to the ambient temperature due to direct exposure to the environment. The highest temperature in the LCZ was reported in June, corresponding to the peak solar irradiation, and reached 363.63 K. The SGSP generates at least 29.6 kWh/day of thermal energy, which is almost 2.73 times the daily thermal energy requirement of a household.

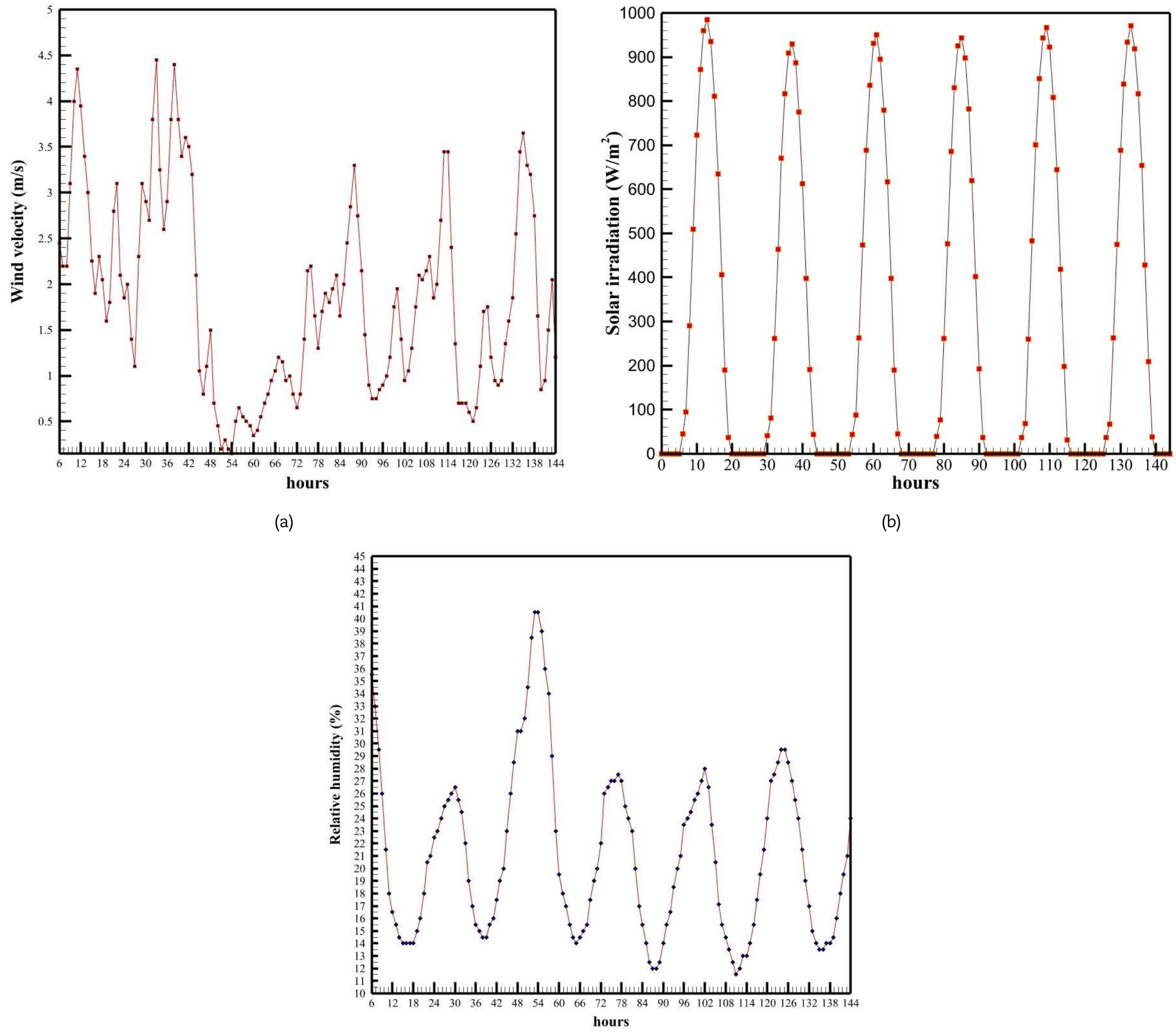

Fig. 12. Hourly variations of weather conditions from June 22 to June 27, (a) Wind velocity, (b) Solar irradiation, (c) Relative humidity.

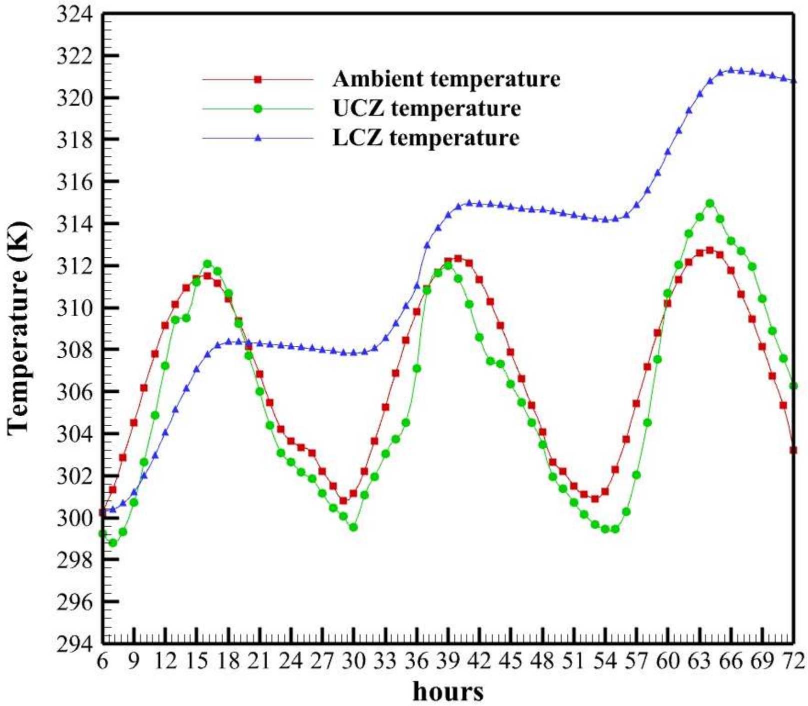

Fig. 13. Hourly variations of ambient temperature, UCZ, and LCZ temperatures from June 22 to June 24.

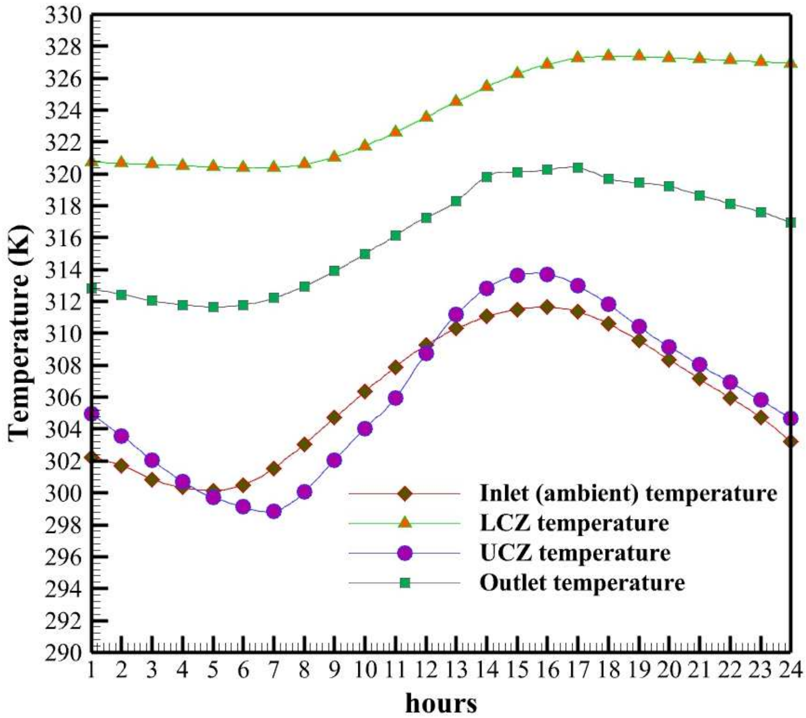

Fig. 14. Hourly variations of ambient temperature, outlet fluid temperature, and the LCZ and UCZ temperatures on June 24.

Table 8. Specifications of the solar pond.

Parameter	Value	Parameter	Value
X_g	2 m	$C_{p,lcz}$ [31]	3300 J/kg K
$C_{p,ucz}$ [26]	4180 J/kg K	T_{ground}	291.52 K
ρ_{ucz} [26]	1000 kg/m^3	ρ_{lcz} [31]	1200 kg/m^3
L_t	30 m	k_i [49]	0.035 W/m.K
k_g [26]	2.5 W/m.K	k_w [26]	0.596 W/m.K
k_{pipe}	400 W/m.K	m_i	80 kg/hr
D_o	0.02 m	D_i	0.016 m

6.3. SSS

To meet the freshwater demand of a four-person household, a SSS with a glass cover area of 9 m^2 was designed. In this system, 28 steps are used, each with a length of 2.5 meters, a height of 2.5 centimeters, and a floor of 10 centimeters. Extruded polystyrene foam was used as insulation. The monthly performance of the active and passive SSS, with an inlet flow rate of 80 kg/h, was evaluated using Table 9. Monthly variations in freshwater production and outlet temperature for both active and passive SSS are shown in Fig. 16. The quantity of freshwater produced in the cogeneration system consisting of a PV/T collector, a SGSP, and a SSS is higher than in other configurations. Therefore, placing the SGSP before the SSS can result in a minimum daily production of 12.5 liters of freshwater, which is 1.3 liters more than the daily freshwater requirement of a four-person household. The highest amount of freshwater production occurs in June due to the highest levels of solar irradiation and the high inlet temperature of the SSS. The temperature of the salinewater output and the amount of freshwater produced are higher when the SSS is coupled with the SGSP and the PV/T compared to other configurations. This is while the highest and lowest temperatures of the produced hot water are 367.15 K and 307.71 K, respectively, occurring in June and January.

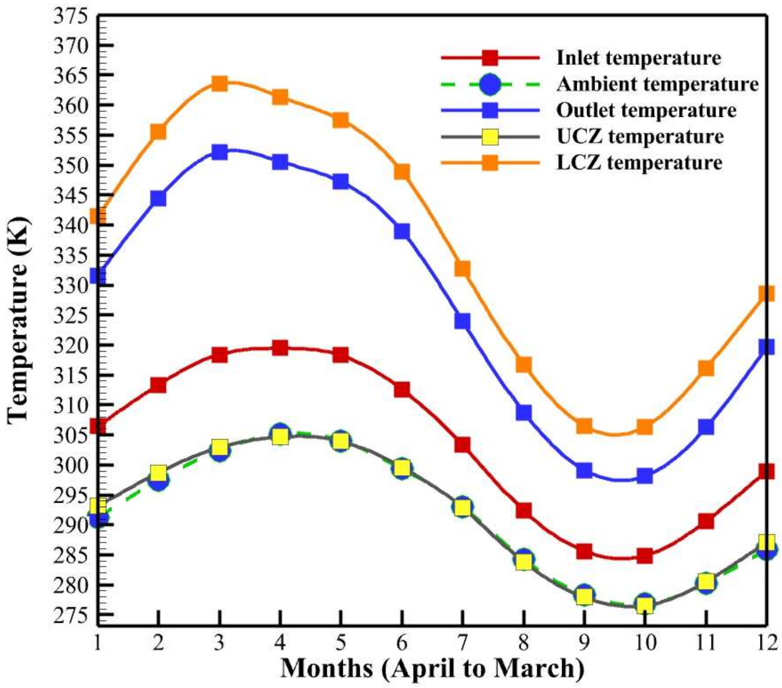

Fig. 15. Monthly temperature variations of the LCZ, saline water entry, and exit of the heat exchanger.

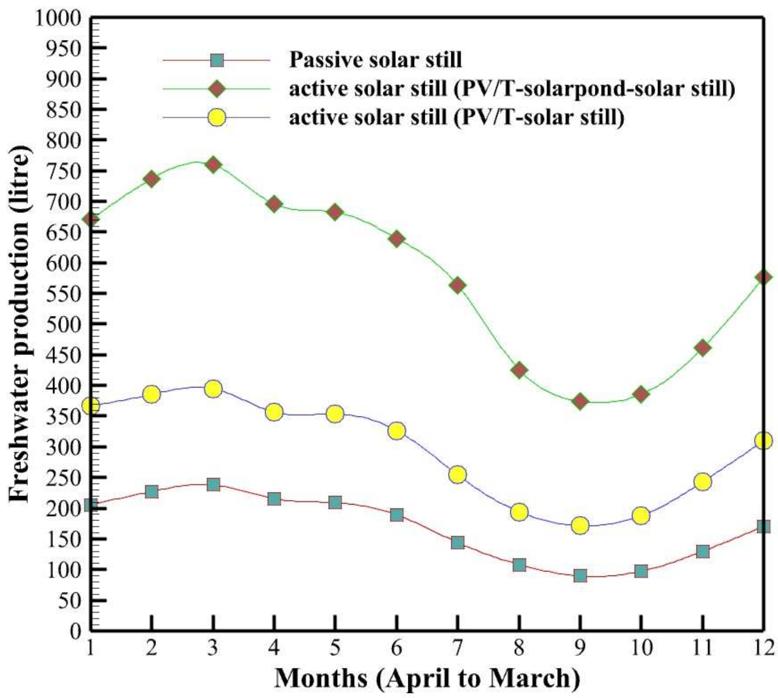

(a)

Fig. 16. Monthly variations in (a) freshwater production and (b) brine outlet temperature of passive and active SSSs.

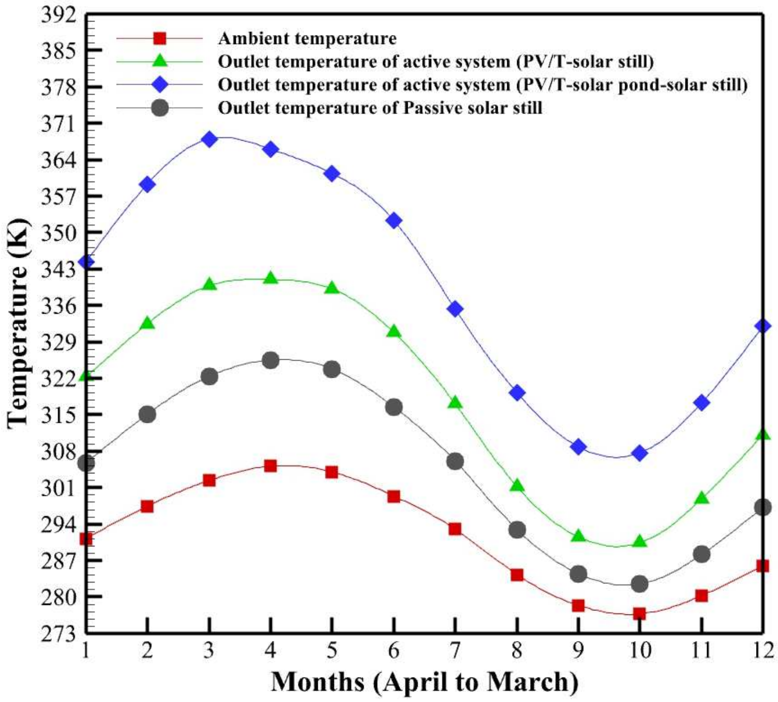

(b)

Fig. 16. Continued.

The cogeneration system exhibits excellent thermal performance, such that it increased the outlet fluid temperature to more than nine times the inlet fluid temperature during January. According to Fig. 17, this system is capable of producing at least 63.67 kWh/day of heat in the coldest month of January. The seasonal trend of heat production shown in the figure arises from the competition among three main climatic factors: solar radiation (positive driver), ambient temperature (dual effect on absorption and losses), and wind speed (loss enhancer). From April to June, the gradual increase in solar radiation and ambient temperature dominates over the concurrent rise in wind speed, leading to an upward trend in heat production. From July to September, although solar radiation remains appreciable, ambient temperature reaches its peak, reducing the effective temperature difference for heat absorption; meanwhile, wind speed stays high, and together these factors cause a declining trend in heat production. From October to December, the sharp drop in solar radiation combined with decreasing ambient temperature cannot be compensated by the simultaneous reduction in wind speed, so heat production falls to its lowest level. From January to March, the rapid increase in solar radiation together with the gradual rise in ambient temperature—which lowers convective losses—restores the upward trend in heat production, with a steeper slope toward the end of this period as solar radiation intensifies near the spring equinox. Overall, heat production is governed by the interplay of solar radiation (positive), ambient temperature (reducing losses at moderate levels but narrowing the absorption driving force at very high levels), and wind speed (increasing losses). The seasonal variations of these three parameters determine the observed annual pattern.

6.4. Daily performance of the solar cogeneration system

Here, to better understand the operation of this solar cogeneration system, its hourly performance is tested on April 1st. The weather conditions are shown in Fig. 18. The weather data presented were extracted from the Meteonorm 7.3 software [43]. The areas of the PV/T, the SSS, and the SGSP are 21 m², 9 m², and 10 m², respectively.

According to Figs. 19 and 20, during the hours when there is no solar irradiation, the fluid exiting the PV/T, which is at ambient temperature, absorbs heat from the SGSP, resulting in freshwater production in the SSS. As illustrated in Fig. 19, unlike the other hours of the day, the outlet temperature from the SSS is lower than the inlet temperature due to the absence of solar irradiation and heat loss to the environment. The SGSP performs well at night, and in the absence of solar irradiation, the production of freshwater and hot water continues. Despite the high solar irradiation at 12:00 PM, the system experiences a reduction in freshwater and energy production from 1:00 PM to 4:00 PM due to the sudden onset of cloud cover, which leads to a decline in solar irradiation. Subsequently, around 4:00 PM, as the weather conditions improve and solar irradiation rises again, freshwater and energy production reach their maximum levels of the entire day.

Table 9. Parameters related to SSS modeling [33-41].

Parameter	Value	Parameter	Value
α_w	0.05	ε_w	0.96
E	15 m^{-1}	α_b	0. 95
ε_g	0.88	δ_{glass}	4 mm
τ_w	0.95	$h_{c,b-w}$	135 W/m²K
k_i [49]	0.028 W/m.K	L_i	0.02 m

The SGSP is capable of providing a stable thermal output, which is crucial for maintaining the efficiency of the system. Due to the limited or absence of solar irradiance during nighttime hours, the production of freshwater and thermal energy during these periods experiences only minimal variation. During these hours, electricity generation also drops to zero. This cogeneration system is capable of producing 58.51 liters of freshwater, 7.123 kWh of electricity, and 68.425 kWh of heat on April 1st, of which 21.68 liters of freshwater and 17.98 kWh of the heat are generated during the night. The simultaneous utilization of solar energy and thermal storage enables the continuous fulfillment of heating and freshwater demands throughout the year, thereby enhancing the system's stability. Based on the above results, this cogeneration system can provide a sustainable future and improve the quality of life in regions with high demand for electricity, heat, and freshwater.

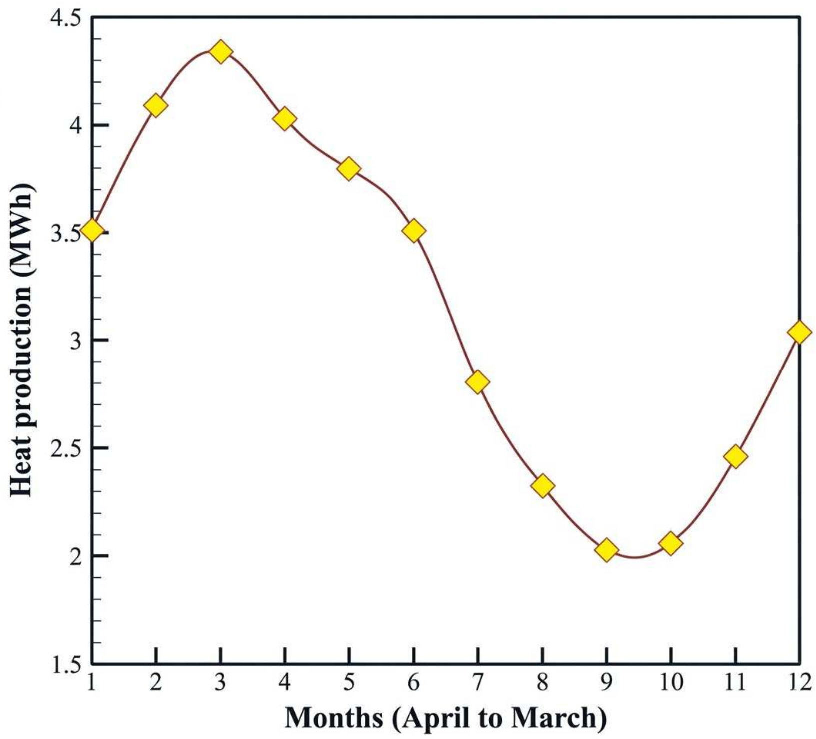

Fig. 17. Monthly variations of the produced thermal energy.

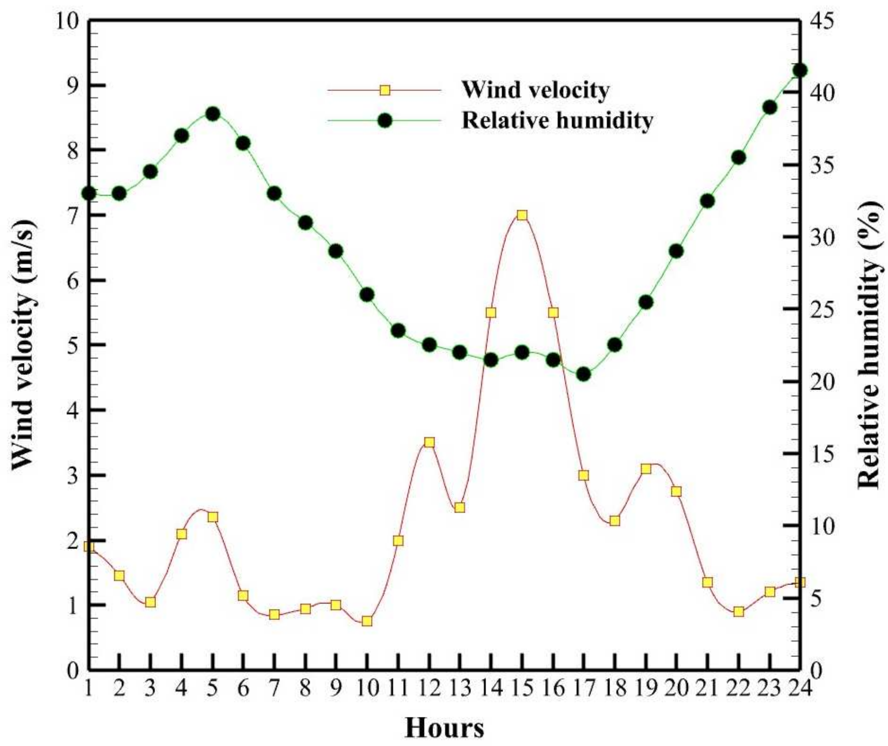

Fig. 18. Hourly variations of weather conditions on April 1st.

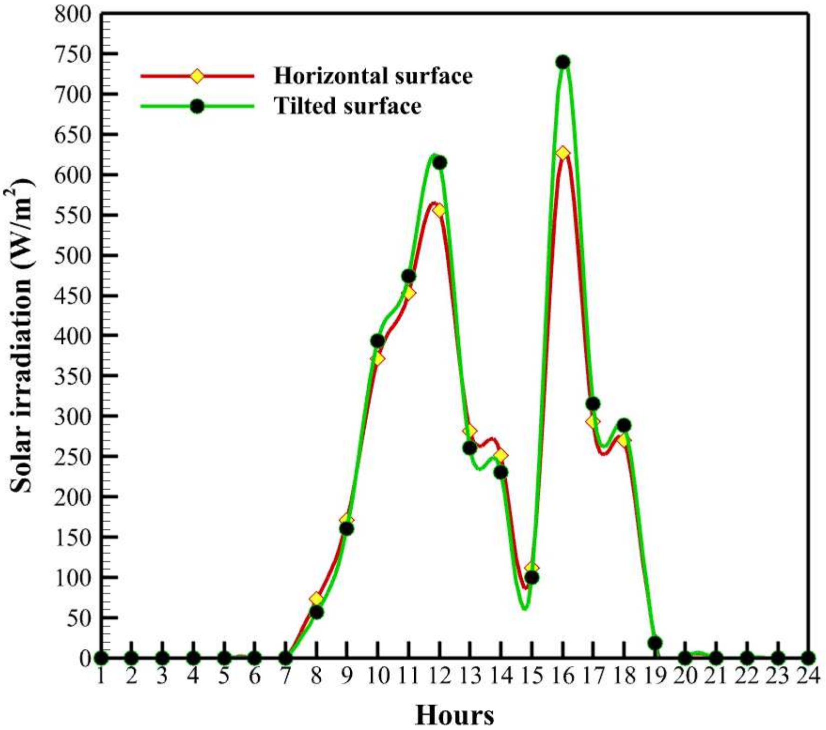

(b)

Fig. 18. Continued.

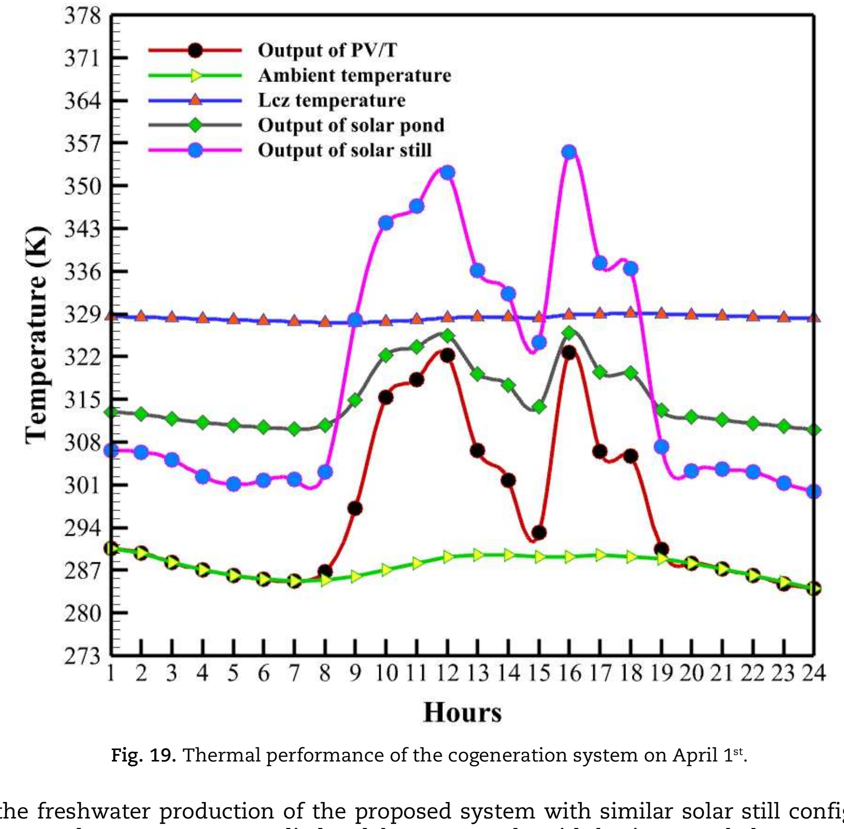

Fig. 19. Thermal performance of the cogeneration system on April 1st.

Table 10 compares the freshwater production of the proposed system with similar solar still configurations reported in the literature. Most of the reported systems were studied at laboratory scale with basin areas below 0.75 m², whereas the present system considers a larger scale of 7 m². The proposed system achieves a specific freshwater productivity of 8.36 L m^{-2} day^{-1}, which is higher than the values reported in previous studies (typically ranging from 1.91 to 5.33 L m^{-2} day^{-1}). In addition to the specific productivity, the total freshwater yield of the proposed system reaches 58.51 L day^{-1}, whereas the reported small-scale systems typically produce a maximum of about 2.57 L day^{-1} due to their limited absorber area. Furthermore, the integration of the SGSP enables thermal energy storage and extends freshwater production beyond sunshine hours. The system is specifically designed as a trigeneration configuration to simultaneously produce freshwater, electrical power, and useful thermal energy, and is not limited to freshwater production alone. Overall, the results demonstrate that the proposed system exhibits superior freshwater production performance compared with similar systems reported in the literature.

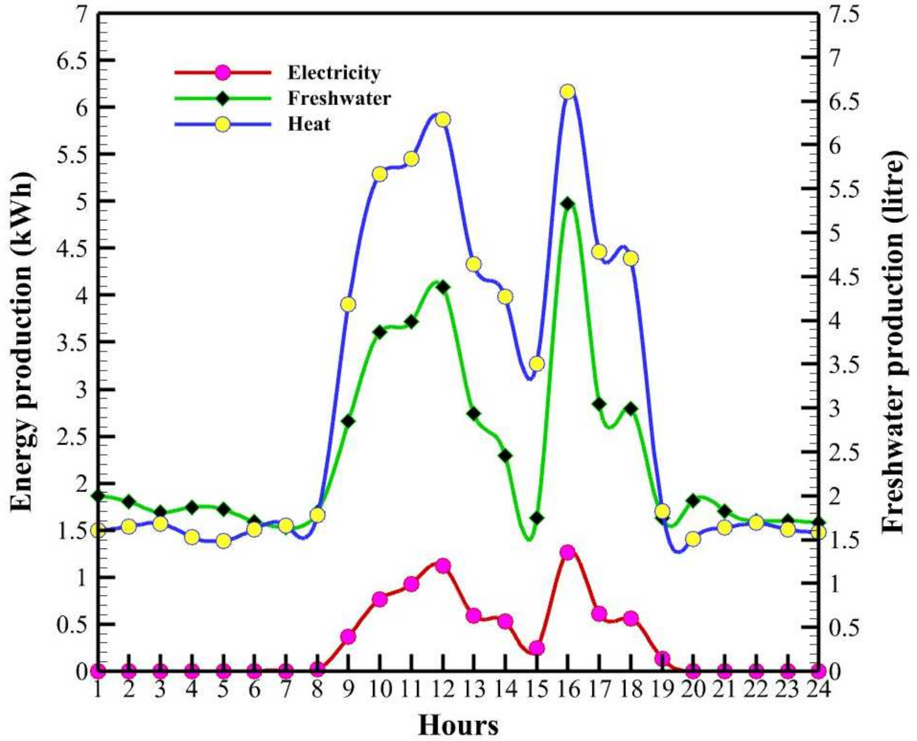

Fig. 20. Hourly production of electricity, freshwater and heat by the cogeneration system on April 1st.

Table 10. Comparison of freshwater productivity with previous studies.

Refrence	Type of solar still	Integrated enhancement techniques	Evaporation Basin area (m^2)	Specific freshwater productivity (L/m^2day)
Asadabadi and Sheikholeslami [6]	Pyramid	Hollow copper fins + glass wool insulation	0.25	5.33
Aghakhani et al. [7]	Single slope stepped	Thermoelectric module (hot side heater + cold side condenser)	-	1.91
Prakash and Kumar [8]	Single slope stepped	Internal reflectors + external reflector + glass cooling	0.75	3.43
Taheri Mousavi [9]	Hemispherical funnel stepped	Funnel stepped absorber plate	0.256	4.61
Pandey and Naresh [10]	Pyramid	Pulsating heat pipe (PHP)	0.49	4.1
Mohtasim et al. [14]	Pyramid	PVT/HNPCM/Fin	0.25	4.109
Rajesh and Chiranjeevi [15]	Single slope stepped	Bi-directional serpentine PVT absorber	0.45	3.46
Present study	Stepped	Header-riser PVT collector + SGSP	7	8.3586

7. Conclusions

The operation of buildings contributes to approximately 30% of the world's final energy consumption and accounts for 26% of greenhouse gas emissions related to energy. Among these emissions, 8% come directly from building activities, while the remaining 18% are produced indirectly through the generation of electricity and heat used by buildings. [50]. At the same time, domestic or municipal water consumption accounts for approximately 12% of global freshwater withdrawals, highlighting the significant contribution of households to overall water demand [51]. These challenges highlight the need for small-scale, solar-based cogeneration systems for electricity, heat, and freshwater, aimed at improving living quality and ensuring sustainable energy and water supply in remote areas. In this study, for the first time, a small-scale cogeneration system based on a photovoltaic-thermal (PV/T), a salt gradient solar pond (SGSP), and a stepped solar still (SSS) was designed for sustainable and clean production of energy and freshwater in arid remote areas. Mathematical models were developed and validated in EES software to evaluate the performance of each component of the system. Subsequently, the cogeneration system for electricity, fresh water, and heat was designed to supply the needs of a four-person household under the climatic conditions of Semnan city. The results of the present study are as follows:

- The electricity produced by the glazed PV/T showed a significant difference compared to that produced by the unglazed PV/T. The unglazed PV/T, with an area of 21 m^2, supplied at least 6.28 kWh/day of electricity and generated an average annual surplus of 1.58 MWh beyond the household's consumption.
- The monthly thermal performance of the SGSP coupled with the PV/T was evaluated. In January, the coldest month with an ambient temperature of 276.77 K, the 10 m^2 SGSP coupled with the PV/T demonstrated strong performance, raising the temperature of the fluid exiting the PV/T (12.5 °C) collector to more than twice its original value (26 °C).
- Throughout the year, the UCZ temperature remained near the ambient level, while the highest temperature in the LCZ is 363.63 K in June, corresponding to the peak in solar irradiation.
- The cogeneration system combining a PV/T, a SGSP, and a SSS delivers 3.429 m^3 of freshwater more than a system based only on a PV/T and a SSS.
- In this cogeneration system, the areas of the PV/T collector, the SSS, and the SGSP are 21 m^2, 9 m^2, and 10 m^2, respectively. The cogeneration system is capable of producing annually 4.026 MWh of electricity, 6.972 m^3 of fresh water, and 37.99

MWh of heat. The proposed system is also capable of producing, daily, at least 12.5 liters of fresh water, 67.63 kWh of heat, and 6.284 kWh and 12.14 kWh of electricity during the cold and warm seasons, respectively.

– Hourly simulation of the cogeneration system's performance on April 1st, under the climatic conditions of Semnan, showed that the system can produce 58.81 liters of fresh water, 7.123 kWh of electricity, and 68.425 kWh of heat per day. Interestingly, 21.68 liters of fresh water and 17.98 kWh of heat were produced during the night.

Author Contributions

M. Bostani conducted the simulations and analyzed the results; R. Rafee planned the scheme, initiated the project, and suggested the simulations; S. Rashidi suggested the numerical method and checked the model validation. The manuscript was written through the contribution of all authors. All authors discussed the results, reviewed the manuscript, and approved the final version.

Acknowledgments

Not applicable.

Conflict of Interest

The authors declared no potential conflicts of interest concerning the research, authorship, and publication of this article.

Funding

The authors received no financial support for the research, authorship, and publication of this article.

Data Availability Statements

Not applicable.

Nomenclature

A_b	Absorber area [m²]
A_c	Area of PV/T [m²]
A_g	Glass cover area [m²]
A_{lcz}	Area of the lower convective zone [m²]
A_{ucz}	Area of the upper convective zone [m²]
A_w	Evaporation area [m²]
C_p	Heat capacity of saline water [J/kg.K]
C_b	Bond conductance [W/m.K]
$C_{p.lcz}$	Specific heat capacity of the lower convective zone [J/kg.K]
$C_{p.ucz}$	Specific heat capacity of the upper convective zone [J/kg.K]
D_i	Tube inside diameter [m]
D_h	Header pipe diameter [m]
D_o	Tube outside diameter [m]
E	Extinction coefficient [m⁻¹]
h_b	Heat transmission coefficient between the bottom surface of the steps and the ambient [W/m².K]
$h_{c,b-w}$	Heat transmission coefficient between the bottom surface of the steps and the saline water [W/m².K]
h_i	Enthalpy of inlet saline water [J/kg]
h_o	Enthalpy of outlet saline water[J/kg]
I_t	Solar intensity [W/m²]
I_x	Absorbed irradiation at depth x [W/m²]
k_{back}	PV/T back insulation conductivity [W/m.K]
k_{edge}	PV/T edge insulation conductivity [W/m.K]
k_g	The ground conductivity [W/m.K]
k_i	Insulation material conductivity [W/m.K]
k_{pipe}	Thermal conduction of the heat exchanger pipes in the solar pond [W/m.K]
k_{plate}	Thermal conductivity of the PV/T absorber plate [W/m.K]
k_{si}	Thermal conductivity of silicon [W/m.K]
k_w	Thermal conductivity of saline water [W/m.K]
L	Pond depth [m]
L_i	Insulation thickness [m]
L_{lcz}	Thickness of the lower convective zone [m]
L_s	PV/T collector length [m]
L_{ucz}	Thickness of the lower convective zone [m]
L_t	Length of the heat exchanger pipe at the bottom of the pond [m]
L_{ucz}	Thickness of the upper convective zone [m]
Q_{b-a}	Heat loss from the bottom surface of the steps to the ambient [W]
$Q_{c.b-w}$	Convection heat transmission between steps and saline water [W]
$Q_{c.g-sky}$	Convection heat transmission between the glass and the sky [W]
$Q_{c.w-g}$	Convective heat transmission between the water and the glass [W]
Q_{cond}	Conduction heat transmission rate from LCZ to UCZ [W]
Q_e	Electricity production of the PV/T [W]
$Q_{e.w-g}$	Evaporative heat transmission between water and glass [W]
Q_{ground}	LCZ loss to the ground [W]
Q_{load}	Absorption heat rate from LCZ [W]
$Q_{losses.ucz}$	Overall heat rate from UCZ to ambient [W]
$Q_{r.g-sky}$	Radiative heat transmission between the glass and the sky [W]
$Q_{r.w-g}$	Radiative heat transfer between the water and the glass [W]
Q_u	Thermal energy gained by PV/T [W]
S	Absorbed irradiation [W/m²]
t	Thickness of pipe wall [m]
T_a	Ambient temperature [K]
T_{ground}	Ground temperature [K]
T_i	Entry temperature [K]
T_{ref}	Reference temperature [K]
T_w	Saline water temperature [K]
U_{ca}	Heat loss coefficient between the PV cells and the absorber [W/m².K]
U_e	Edge heat loss coefficient of PV/T [W/m².K]
$\bar{U}_L$	Modified heat loss coefficient of PV/T [W/m².K]
U_{LS}	Overall heat transfer coefficient water to ambient [W/m².K]
W	Tube spacing [m]
w_c	PV/T Collector width [m]
X_g	Depth of water table [m]
Greek letters	
ε_p	PV/T absorber plate emissivity
ε_g	Glass cover emissivity
ε_w	Water emissivity
δ_a	Absorber plate thickness [m]
δ_{back}	PV/T back insulation thickness [m]
δ_{edge}	PV/T edge insulation thickness [m]
δ_{glass}	Glass cover thickness [m]

$\dot{m}$	Inlet mass flow rate to the collector [kg/s]	α_p	Absorptivity of the PV/T absorber plate
$\dot{m}_{evap}$	Freshwater production rate [kg/hr]	α_b	Solar absorptivity of the steps
$\dot{m}_i$	Inlet mass flow rate [kg/s]	α_g	Glass absorptivity
$\dot{m}_o$	Outlet mass flow rate [kg/s]	α_w	Water Absorptivity
$\dot{m}_w$	Saline water mass flow rate on solar still steps [kg/hr]	a'_b	The fractions of solar irradiation absorbed by the steps of the solar still
N_c	Numbers of PV/T collectors	a'_w	The fractions of solar irradiation absorbed by the saline water
β_{ref}	Cell efficiency temperature coefficient [1/k]	**Subscript**	
β	Collector slope, degree	HNPCM	Hybrid nano-Phase change material
τ_g	Glass transmissivity	LCZ	Lower convection zone
τ_w	Water transmissivity	MCSSS	Modified concatenated stepped solar still
η_{ref}	Electrical efficiency for the reference temperature	NCZ	Non-convection zone
τ_α	Transmissivity based on absorption	PV	Photovoltaic panel
τ_r	Transmissivity based on reflection- refraction	PV/T	Photovoltaic-thermal
d_t	Time step [s]	SGSP	Salt gradient solar pond
ρ	Density [kg/m^3]	SS	Solar still
δ_{si}	Thickness of silicon [m]	SSS	Stepped solar still
δ_p	Collector thickness [m]	UCZ	Upper convection zone

References

[1] Mahmoudi, A., Bostani, M., Rashidi, S., Valipour, M.S., Challenges and opportunities of desalination with renewable energy resources in Middle East countries, *Renewable and Sustainable Energy Reviews*, 184, 2023, 113543.

[2] Al-Rashed, A.A.A.A., Oztop, H.F., Kolsi, L., et al., CFD study of heat and mass transfer and entropy generation in a 3D solar distiller heated by an internal column, *International Journal of Mechanical Sciences*, 152, 2019, 280-288.

[3] Çakmak, F.A., Selimefendigil, F., Öztop, H.F., A review on different Nano-Enhanced techniques for productivity improvement of solar stills, *Thermal Science and Engineering Progress*, 55, 2024, 103006

[4] Goshayeshi, H.R., Chaer, I., Yebiyo, M., Öztop, H.F., Experimental investigation on semicircular, triangular and rectangular shaped absorber of solar still with nano-based PCM, *Journal of Thermal Analysis and Calorimetry*, 147(4), 2022, 3427-3439.

[5] Esmaeili, Z., Sheikholeslami, M., Enhancing solar still productivity through glass cover geometry and internal baffle design: A numerical approach, *Journal of Water Process Engineering*, 83, 2026, 109541.

[6] Asadabadi, M.J.R., Sheikholeslami, M., Impact of Utilizing Hollow Copper Circular Fins and Glass Wool Insulation on the Performance Enhancement of Pyramid Solar Still Unit: An Experimental Approach, *Solar Energy*, 241, 2022, 564-575.

[7] Aghakhani, S., Kavehfarsani, M., Pordanjani, A.H., Afrand, M., Energy and exergoeconomic analysis of solar stills integrated with thermoelectric technology: A case study on environmental and economic sustainability, *Renewable Energy*, 239, 2025, 121989.

[8] Prakash, A., Kumar, M., Experimental investigations on simple and modified concatenated stepped solar still units for the extraction of clean water: A comparative study, *Renewable Energy*, 238, 2025, 121957.

[9] Taheri Mousavi, S.M., Investigation of the effect of different absorber plate configurations of hemispherical solar still, *Renewable Energy*, 237(PB), 2024, 121660.

[10] Pandey, N., Naresh, Y., A comprehensive 4E (energy, exergy, economic, environmental) analysis of novel pyramid solar still coupled with pulsating heat pipe: An experimental study, *Renewable Energy*, 225(C), 2024, 120227.

[11] Bostani, M., Rafee, R., Rashidi, S., Potential and challenges of solar-based cogeneration systems for decentralized production of power, heat, and freshwater in rural MENA regions, *Energy Conversion and Management: X*, 30, 2026, 101732.

[12] Sheikholeslami, M., Yarmohamad, S., Numerical analysis and performance optimization of a solar photovoltaic–electrolyzer system with hybrid nanofluid-based cooling for sustainable hydrogen production, *Renewable Energy*, 268, 2026, 125526.

[13] Manokar, A.M., Winston, D.P., Kabeel, A.E., El-Agouz, S.A., Sathyamurthy, R., Arunkumar, T., Madhu, B., Ahsan, A., Integrated PV/T Solar Still - A Mini-Review, *Desalination*, 435, 2018, 259-267.

[14] Mohtasim, M.S., Kibria, M.G., Pranto, M.M.H., Das, B.K., Hybrid PVT integrated pyramid solar still: 11E, sustainability, and sustainable development goals assessment, *Renewable Energy*, 246, 2025, 122914.

[15] Rajesh, S., Chiranjeevi, C., Experimental investigations on a sustainable cogeneration system for power and desalination with 4-E analysis, *Solar Energy*, 264, 2023, 112046.

[16] Hill, J.E., Streed, E.R., A method of testing for rating solar collectors based on thermal performance, *Solar Energy*, 18(5), 1976, 421-429.

[17] Florschuetz, L.W., Extension of the Hottel-Whillier model to the analysis of combined photovoltaic/thermal flat plate collectors, *Solar Energy*, 22(4), 1979, 361-366.

[18] Charalambous, P.G., Kalogirou, S.A., Maidment, G.G., Yiakoumetti, K., Optimization of the photovoltaic thermal (PV/T) collector absorber, *Solar Energy*, 85(5), 2011, 871-880.

[19] Kalogirou, S.A., *Solar Energy Engineering: Processes and Systems*, 2nd ed., Academic Press, Cambridge, MA, 2014.

[20] Duffie, J.A., Beckman, W.A., *Solar Engineering of Thermal Processes*, 4th ed., John Wiley & Sons, Hoboken, New Jersey, 2013.

[21] Sukhatme, S., Nayak, J., *Solar Energy: Principles of Thermal Collection and Storage*, 3rd ed., Tata McGraw Hill, New York, 2009.

[22] Al-Waeli, A.H.A., Kazem, H.A., Chaichan, M.T., Sopian, K., *Photovoltaic/Thermal (PV/T) Systems: Principles, Design, and Applications*, Springer, Cham, 2019.

[23] Holman, J.P., *Heat Transfer (SI Units)*, 9th ed., Tata McGraw-Hill, New Delhi, 2008.

[24] Tiwari, G.N., *Solar Energy: Fundamentals, Design, Modelling and Applications*, Alpha Science International, Pangbourne, England, 2002.

[25] Sayer, A.H., Al-Hussaini, H., Campbell, A.N., New theoretical modelling of heat transfer in solar ponds, *Solar Energy*, 125, 2016, 207-218.

[26] Chakrabarty, S.G., Wankhede, U.S., Shelke, R.S., Gohil, T.B., Investigation of temperature development in salinity gradient solar pond using a transient model of heat transfer, *Solar Energy*, 202, 2020, 32-44.

[27] Jaefarzadeh, M.R., Heat Extraction from a Salinity-Gradient Solar Pond Using in Pond Heat Exchanger, *Applied Thermal Engineering*, 26(16), 2006, 1858-1865.

[28] Green, D.W., Southard, M.Z., *Perry's Chemical Engineers' Handbook*, 9th ed., McGraw-Hill, New York, 2018.

[29] Verma, S., Das, R., Transient study of a solar pond under heat extraction from non-convective and lower convective zones considering finite effectiveness of exchangers, *Solar Energy*, 223, 2021, 437-448.

[30] Abdullah, A.L., Misha, S., Tamaldin, N., Rosli, M.A., Sachit, F.A., A Review: Parameters Affecting the PVT Collector Performance on the Thermal, Electrical, and Overall Efficiency of PVT System, *Journal of Advanced Research in Fluid Mechanics and Thermal Sciences*, 60(2), 2019, 191-232.

[31] Lu, H.M., Walton, J.C., Swift, A.H.P., Desalination coupled with salinity-gradient solar ponds, *Desalination*, 136(1-3), 2001, 13-23.

[32] Zarei, M., Rashidi, S., Rafee, R., Li, G., Sustainable freshwater production using novel cascade solar still with phase change material, serpentine water path, and copper fins, *Environmental Science and Pollution Research*, 31(11), 2024, 16928-16939.

[33] Dashtban, M., Tabrizi, F.F., Thermal analysis of a weir-type cascade solar still integrated with PCM storage, *Desalination*, 279(1-3), 2011, 415-422.

[34] El-Sebaii, A.A., Al-Ghamdi, A.A., Al-Hazmi, F.S., Faidah, A.S., Thermal performance of a single basin solar still with PCM as a storage medium, *Applied Energy*, 86(7-8), 2009, 1187-1195.

[35] Zurigat, Y.H., Abu-Arabi, M.K., Modelling and performance analysis of a regenerative solar desalination unit, *Applied Thermal Engineering*, 24(7), 2004, 1061-1072.

[36] Abujazar, M.S., Fatihah, S., Ibrahim, I.A., Kabeel, A.E., Sharil, S., Productivity Modelling of a Developed Inclined Stepped Solar Still System Based on Actual Performance and Using a Cascaded Forward Neural Network Model, *Journal of Cleaner Production*, 170, 2018, 147-159.
[37] Velmurugan, V., Senthil Kumaran, S., Niranjan Prabhu, V., Srithar, K., Productivity Enhancement of Stepped Solar Still: Performance Analysis, *Thermal Science*, 12(3), 2008, 153-163.
[38] Alaudeen, A., Johnson, K., Ganasundar, P., Abuthahir, A.S., Srithar, K., Study on Stepped Type Basin in a Solar Still, *Journal of King Saud University-Engineering Sciences*, 26(2), 2014, 176-183.
[39] El-Samadony, Y.A., El-Maghlany, W.M., Kabeel, A.E., Influence of glass cover inclination angle on radiation heat transfer rate within stepped solar still, *Desalination*, 384, 2016, 68-77.
[40] Velmurugan, V., Naveen Kumar, K.J., Noorul Haq, T., Srithar, K., Performance analysis in stepped solar still for effluent desalination, *Energy*, 34(9), 2009, 1179-1186.
[41] Abujazar, M.S.S., Fatihah, S., Lotfy, E.R., Kabeel, A.E., Sharil, S., Performance evaluation of inclined copper-stepped solar still in a wet tropical climate, *Desalination*, 425, 2018, 94-103.
[42] Sepehr, M., Eghtedaei, R., Toolabimoghadam, A., Noorollahi, Y., Mohammadi, M., Modeling the electrical energy consumption profile for residential buildings in Iran, *Sustainable Cities and Society*, 41, 2018, 481-489.
[43] Meteotest, *User Manual of Meteonorm 7.3 Software*, Meteotest, Bern, Switzerland, 2019.
[44] Lévesque, B., Lavoie, M., Joly, J., Residential water heater temperature: 49 or 60 degrees Celsius?, *Canadian Journal of Infectious Diseases*, 15(1), 2004, 11-12.
[45] Ali, M., Terfa, A.B., State of water supply and consumption in urban areas at household level: A case study of East Wollega Zone, Ethiopia, *British Journal of Humanities and Social Sciences*, 5(2), 2012, 1-15.
[46] Carpino, C., Bruno, R., Bevilacqua, P., Arcuri, N., *Are ICFs Suitable Building Envelope Solutions for Mediterranean Climatic Conditions? A Critical Analysis Concerning Thermal Properties and Annual Energy Performances*, Building Simulation 2019: 16th Conference of IBPSA, Rome, Italy, BS2019_211036, 2019, 480-487.
[47] Bostani, M., Rafee, R., Rashidi, S., Li, G., Efficient salt gradient solar pond for thermal energy storage - A study on environment-friendly insulation materials, *Journal of Energy Storage*, 129, 2025, 117337.
[48] Tsilingiridis, G., Papakostas, K., Investigating the relationship between air and ground temperature variations in shallow depths in northern Greece, *Energy*, 73, 2014, 1007-1016.
[49] Özlüsoylu, I., Istek, A., *The Effect of Hybrid Resin Usage on Thermal Conductivity in Ecological Insulation Panel Production*, 4th International Conference on Engineering Technology and Applied Sciences (ICETAS), Kiev, Ukraine, 2019.
[50] *International Energy Agency, Tracking Buildings 2022*, IEA Publications, Paris, France, 2022.
[51] *UNESCO, The United Nations World Water Development Report 2024: Water for Prosperity and Peace*, UNESCO, Paris, 2024.

ORCID iD

Mohammad Bostani https://orcid.org/0009-0000-1219-4429
Roohollah Rafee https://orcid.org/0000-0002-4289-3420
Saman Rashidi https://orcid.org/0000-0001-6266-920X
Guiqiang Li https://orcid.org/0009-0000-0605-6900

How to cite this article: Bostani M., et al. Numerical Investigation on a Novel Solar-Based Cogeneration System for Sustainable Power, Heat, and Freshwater Production in Remote Residential Buildings, *J. Appl. Comput. Mech.*, xx(x), 2026, 1–22. https://doi.org/10.22055/jacm.2026.49245.5832